INTERNATIONAL JOURNAL FOR NUMERICAL METHODS IN FLUIDS
Int. J. Numer. Meth. Fluids 2006; **52**:119–162
Published online 10 February 2006 in Wiley InterScience (www.interscience.wiley.com). DOI: 10.1002/fld.1171

k-Version of finite element method in 2-D polymer flows: Oldroyd-B constitutive model

K. S. Surana[1,*,†], A. Mohammed[1], J. N. Reddy[2] and P. W. TenPas[1]

[1]*The University of Kansas, Department of Mechanical Engineering, 3138 Learned Hall, Lawrence, KS 66044, U.S.A.*
[2]*Texas A & M University, Department of Mechanical Engineering, College Station, TX 47843-3123, U.S.A.*

SUMMARY

In this paper, a new mathematical framework based on h, p, k and variational consistency (VC) of the integral forms is utilized to develop a finite element computational process of two-dimensional polymer flows utilizing Oldroyd-B constitutive model. Alternate forms of the choices of dependent variables in the governing differential equations (GDEs) are considered and is concluded that u, v, p, τ choice yielding strong form of the GDEs is meritorious over others. It is shown that: (a) since, the differential operator in the GDEs is non-linear, Galerkin method and Galerkin method with weak form are variationally inconsistent (VIC). The coefficient matrices in these processes are non-symmetric and hence may have partial or completely complex basis and thus the resulting computational processes may be spurious. (b) Since the VC of the VIC integral forms cannot be restored through any mathematically justifiable means, the computational processes in these approaches always have possibility of spurious solutions. (c) Least squares process utilizing GDEs in u, v, p, τ (strong form of the GDEs) variables (as well as others) is variationally consistent. The coefficient matrices are always symmetric and positive definite and hence always have a real basis and thus naturally yield computational processes that are free of spurious solutions. (d) The theoretical solution of the GDEs are generally of higher order global differentiability. Numerical simulations of such solutions in which higher order global differentiability characteristics of the theoretical solution are preserved, undoubtedly requires local approximations in higher order scalar product spaces $H^{k,p}(\bar{\Omega}_e)$. (e) LSP with local approximations in $H^{k,p}(\bar{\Omega}_e)$ spaces provide an incomparable mathematical and computational framework in which it is possible to preserve desired characteristics of the theoretical solution in the computational process. Numerical studies are presented for fully developed flow between parallel plates and a lid driven square cavity. M1 fluid is used in all numerical studies. The range of applicability of the Oldroyd-B model or lack of it is examined for both model problems for increasing *De*. A mathematical idealization of the corners where stationary wall meets the lid is presented and is shown to simulate the real physics when the local approximations are in higher order spaces and when $h_d \to 0$. For both model problems shear rate $\hat{\dot{\gamma}}$ is

*Correspondence to: K. S. Surana, The University of Kansas, Department of Mechanical Engineering, 3138 Learned Hall, Lawrence, KS 66044, U.S.A.
†E-mail: kssurana@ku.edu

Contract/grant sponsor: DEPSCOR, AFOSR and WPAFB; contract/grant numbers: F 49620-03-1-0298, F 49620-03-1-0201

Received 12 July 2005
Revised 7 November 2005
Accepted 10 November 2005

Copyright © 2006 John Wiley & Sons, Ltd.

examined in the flow domain to establish validity of the Oldroyd-B constitutive model. Copyright © 2006 John Wiley & Sons, Ltd.

KEY WORDS: Oldroyd-B model; least squares process; variational consistency; lid driven cavity

1. INTRODUCTION

Numerical simulation of viscoelastic fluid flows using Oldroyd-B constitutive model has been of interest for years. There has been significant amount of research work published in this area using numerical schemes based on finite difference methods, finite volume methods, boundary element methods and finite element methods. In the earlier developments, Richards *et al*. [1] presented a solution for Oldroyd-B fluid using finite element technique. In Reference [2], laser doppler technique is used to study flow characteristics in the vicinity of a re-entrant corner. In Reference [3], numerical solutions using finite difference method are obtained for Oldroyd fluid for streaming flow past a rigid sphere and spherical bubble. The authors in Reference [4], use mixed finite element formulation to simulate flow through a U-shaped vessel. Jackson *et al.* [5] carried out a rheometrical study on a series of Boger fluids. In Reference [6], mixed element method for the numerical calculation of viscoelastic fluid flow is used to show that numerical errors in the evaluation of extra-stress tensor have consequences on the other field variables for the flow of Maxwell fluid. However, the damage seems to be limited in Oldroyd-B fluid. For the Oldroyd-B fluid at low shear rates [7], it is shown that the steady and dynamic flow properties of the test fluids used are well represented by the constitutive equations. The studies in Reference [8], exhibit superiority of Oldroyd-B constitutive equations over Maxwell model in predicting the dynamic and steady shear properties of materials. Authors in Reference [9], describe boundary element method for flow through sinusoidally corrugated tube. In Reference [10], finite difference method is used to obtain converged solutions with mesh refinement for high Deborah number. Zheng *et al.* [11] used boundary element method to study flow past a sphere in a cylindrical tube. Planar contraction flow of a viscoelastic flow is studied using finite volume technique in Reference [12]. The authors in Reference [13], used mixed finite volume numerical method for viscoelastic flow in an undulating tube. In Reference [14], authors present finite difference technique for flow in periodically constricted tube. Becker *et al.* [15] studied the unsteady motion of a sphere in a viscoelastic fluid using Lagrangian finite element method. The authors in Reference [16] used decoupled finite difference scheme with time stepping for entry flow calculations of Oldroyd-B fluid. Davis and Devin [17] reported that on corner flows of Oldroyd-B fluid Newtonian-like mathematical solutions exist away from the wall. Saramito [18] presents a θ-scheme algorithm and incompressible finite element method for viscoelastic fluid flow. Hulsen *et al*. [19] simulates viscoelastic flows using Brownian configuration fields. In Reference [20] a flux difference splitting scheme is used to approximate the resulting set of equations. Authors in Reference [21] used finite volume method for flow through planar contractions. The authors in Reference [22] reported inertial effect on stability of cone and plate flow. Oliviera *et al.* [23] presents collocation finite volume method for the entry flow problem. Wang *et al.* [24] used higher order upwind finite volume method for contraction flow. We remark that there are many publications up to date than cited here reporting finite element methods for polymer flows, however, the central methodology in the majority of

Copyright © 2006 John Wiley & Sons, Ltd.

these is Galerkin method with weak form with unwinding in some form or the other. Many such works have already been discussed. In view of the fact that our work demonstrates Galerkin method with weak form to be variationally inconsistent and problem dependent due to the use of upwinding methods, citations of more of such works is of little significance here.

While on the surface it appears that a whole host of computational methods have been investigated and published using finite element processes for Oldroyd-B fluid, but upon closer examination we find that the basis behind majority of published formulations is Galerkin method with weak form. Secondly, local approximations are always of class C^0 and in most cases of low degree. To this date, a satisfactory resolution of failure of numerical simulations for Oldroyd-B model using finite element method for increasing Deborah number (De) has been less than satisfactory. Furthermore, even in the published work where some success has been achieved, mesh independent solutions are almost non-existent. Whether the failure of the computational processes is due to less than satisfactory computational processes or limitations of the constitutive model for increasing flow rate (and hence Deborah number) is not clear either.

1.1. Scope of the present work

In the work presented in this paper, the investigations and strategies are multi-fold. First, we present a short derivation of Oldroyd-B model and then we examine the Oldroyd-B constitutive model itself and establish if and when the model is capable of producing satisfactory behaviour that conforms to the physics of flow. In the development of the finite element computational process we utilize a more complete and comprehensive mathematical framework presented recently by Surana *et al.* [25–27] based on variationally consistent integral forms and h, p and k as independent computational parameters. We show that this mathematical and associated computational framework can hardly be blamed if and when the failure of the computational process occurs. Use of this framework is essential in lifting the balance from the computational process and instead be able to focus on the anomalies in the constitutive model that may spring up for specific combination of computational and physical parameters resulting in spurious solutions or failure in obtaining numerical solutions. In the present study, we consider two-dimensional steady flow of Oldroyd-B fluid. Fully developed flow between parallel plates and lid driven cavity are used as model problems.

2. OLDROYD-B CONSTITUTIVE MODEL [28]

This constitutive model is constructed using the convected derivatives of stress and strain rate. The construction of this model can be viewed in two different ways. First we note that, since Jeffreys model [28] is known to describe linear viscoelastic behaviour quantitatively, it is used as a basis to generate Oldroyd-B model or convected Jeffreys model by replacing the partial time derivative with the convected time derivative,

$$\hat{\boldsymbol{\tau}} + \lambda_1 \hat{\boldsymbol{\tau}}_{(1)} = -\hat{\eta}_0 (\hat{\boldsymbol{\gamma}}_{(1)} + \lambda_2 \hat{\boldsymbol{\gamma}}_{(2)}) \tag{1}$$

Copyright © 2006 John Wiley & Sons, Ltd.

Another way to view (1) is to note that based on retarded motion expansion [28] rather than using $\hat{\gamma}_{(1)}$ in the upper convected Maxwell model the next logical term to be added to $\hat{\gamma}_{(1)}$ would be $\hat{\gamma}_{(2)}$ with a multiplier λ_2, which would yield (1). In (1), $\hat{\tau}$ is the total stress tensor. In the following we present a discussion of (1) and make many remarks:

(1) This constitutive model contains three constants or parameters: $\hat{\eta}_0$, the zero shear rate viscosity, λ_1, the relaxation time and λ_2, the retardation time.
(2) If $\lambda_2 = 0$, we obtain upper convected Maxwell model.
(3) If $\lambda_1 = 0$, the model simplifies to a second order fluid with vanishing second normal stress coefficient.
(4) If $\lambda_1 = \lambda_2$, the model yields Newtonian fluid behaviour with viscosity $\hat{\eta}_0$.
(5) Discussion presented in Reference [29] regarding upper convected Maxwell model is important and significant in evaluating what can be expected from the Oldroyd-B model in 2-D flows. Since Oldroyd-B model is derived from Maxwell model by incorporating $\hat{\eta}_0\lambda_2\hat{\gamma}_{(2)}$ term on the right side of the Maxwell model. λ_2 provides additional mechanism by which this model can be forced to yield fluid behaviours either closer to or same as Newtonian or closer to or same as Maxwell. The additional physics in the models essentially alters viscous participation, which obviously effects $\boldsymbol{\tau}$ (and thereby elastic response) through constitutive equations. Nonetheless, the basic mechanism of elasticity in this model is exactly same as that in upper convected Maxwell model (UCMM).
(6) Just like UCMM, Oldroyd-B model also contains one constant λ_1 through which elasticity is incorporated in the model. This may be insufficient for two-dimensional elasticity requiring atleast two elastic constants. In terms of the limitations of the model in simulating two-dimensional elastic response,some discussions presented in Reference [29] for UCMM are also applicable to Oldroyd-B model as well.
(7) When simulating fully two-dimensional flows in which all components of the strain rate tensor are non-zero, physically meaningful resolution of the elastic behaviour may require a mechanism which contains atleast two independent elastic constants which is absent in Oldroyd-B model. Use of Oldroyd-B model for such flows: (i) if able to produce results, the resulting behaviour may be erroneous, the extent of which is application dependent as well as dependent on computational and physical parameters; (ii) or may cease to produce results altogether.
(8) Oldroyd-B model like UCMM is meant to simulate behaviour of dilute polymer solutions in which the behaviour is solvent dominated, hence we expect the elastic behaviour to remain less dominant than viscous for all choices of the physical parameters.
(9) Elongation viscosity, first and second normal stress difference versus $\dot{\gamma}$ in simulations and experiments and many other on going issues and investigations related to Oldroyd-B model as well and their validity are issues of interest and concerns in determining its range of applications and choices of physical parameters for which the model performs satisfactorily.

However, in the present work we take Oldroyd-B model in its present form with the understanding of the issues and limitations presented above and concentrate on the development of a finite element computational process that may possibly allow us to investigate when and why h, p, k independent solutions are possible in the present computational framework.

Copyright © 2006 John Wiley & Sons, Ltd.

2.1. Constitutive equations of the Oldroyd-B model

In (1), $\hat{\boldsymbol{\tau}}_{(1)}$, $\hat{\boldsymbol{\gamma}}_{(1)} = \hat{\dot{\gamma}}$ are the first convected derivatives of the stress and strain rate tensor and $\hat{\boldsymbol{\gamma}}_{(2)}$ is the second convected strain rate tensor, defined by

$$\hat{\boldsymbol{\tau}}_{(1)} = \frac{D\hat{\boldsymbol{\tau}}}{D\hat{t}} - ((\hat{\boldsymbol{\nabla}}\hat{\mathbf{U}})^{\mathrm{T}}.\hat{\boldsymbol{\tau}} + \hat{\boldsymbol{\tau}}.(\hat{\boldsymbol{\nabla}}\hat{\mathbf{U}})) \tag{2}$$

or

$$\hat{\boldsymbol{\tau}}_{(1)} = \frac{\partial\hat{\boldsymbol{\tau}}}{\partial\hat{t}} + (\hat{\mathbf{U}}.\hat{\boldsymbol{\nabla}})\hat{\boldsymbol{\tau}} - ((\hat{\boldsymbol{\nabla}}\hat{\mathbf{U}})^{\mathrm{T}}.\hat{\boldsymbol{\tau}} + \hat{\boldsymbol{\tau}}.(\hat{\boldsymbol{\nabla}}\hat{\mathbf{U}})) \tag{3}$$

and

$$\hat{\boldsymbol{\gamma}}_{(2)} = \frac{D\hat{\boldsymbol{\gamma}}_{(1)}}{D\hat{t}} - ((\hat{\boldsymbol{\nabla}}\hat{\mathbf{U}})^{\mathrm{T}}.\hat{\boldsymbol{\gamma}}_{(1)} + \hat{\boldsymbol{\gamma}}_{(1)}.(\hat{\boldsymbol{\nabla}}\hat{\mathbf{U}})) \tag{4}$$

or

$$\hat{\boldsymbol{\gamma}}_{(2)} = \frac{\partial\hat{\boldsymbol{\gamma}}_{(1)}}{\partial\hat{t}} + (\hat{\mathbf{U}}.\hat{\boldsymbol{\nabla}})\hat{\boldsymbol{\gamma}}_{(1)} - ((\hat{\boldsymbol{\nabla}}\hat{\mathbf{U}})^{\mathrm{T}}.\hat{\boldsymbol{\gamma}}_{(1)} + \hat{\boldsymbol{\gamma}}_{(1)}.(\hat{\boldsymbol{\nabla}}\hat{\mathbf{U}})) \tag{5}$$

Substituting these into (1) and noting that for steady motion we have $\partial\hat{\boldsymbol{\tau}}/\partial\hat{t} = 0$ and $\partial\hat{\boldsymbol{\gamma}}_{(1)}/\partial\hat{t} = 0$, we obtain the following for Oldroyd-B constitutive equations:

$$\begin{aligned}&\hat{\boldsymbol{\tau}} + \lambda_1((\hat{\mathbf{U}}.\hat{\boldsymbol{\nabla}})\hat{\boldsymbol{\tau}} - (\hat{\boldsymbol{\nabla}}\hat{\mathbf{U}})^{\mathrm{T}}.\hat{\boldsymbol{\tau}} - \hat{\boldsymbol{\tau}}.(\hat{\boldsymbol{\nabla}}\hat{\mathbf{U}}))\\ &\quad = -\hat{\eta}_0\hat{\boldsymbol{\gamma}}_{(1)} - \hat{\eta}_0\lambda_2((\hat{\mathbf{U}}.\hat{\boldsymbol{\nabla}})\hat{\boldsymbol{\gamma}}_{(1)} - (\hat{\boldsymbol{\nabla}}\hat{\mathbf{U}})^{\mathrm{T}}.\hat{\boldsymbol{\gamma}}_{(1)} - \hat{\boldsymbol{\gamma}}_{(1)}.(\hat{\boldsymbol{\nabla}}\hat{\mathbf{U}}))\end{aligned} \tag{6}$$

2.2. Elastic-viscous stress decomposition

It has been argued [30] that an alternative form of the constitutive equations (6) obtained using elastic viscous stress decomposition is meritorious over (6) in numerical computations. This form of (6) can be obtained by assuming that $\hat{\boldsymbol{\tau}} = \hat{\boldsymbol{\tau}}^e + \hat{\boldsymbol{\tau}}^v$ in which $\boldsymbol{\tau}^e$ is the elastic stress tensor and $\boldsymbol{\tau}^v$ is the viscous stress tensor. Furthermore, $\hat{\boldsymbol{\tau}}^v = -\hat{\eta}_0(\hat{\boldsymbol{\nabla}}\hat{\mathbf{U}} + (\hat{\boldsymbol{\nabla}}\hat{\mathbf{U}})^{\mathrm{T}})$. Substituting for $\boldsymbol{\tau}$ and $\boldsymbol{\tau}^v$ in (6), we obtain the following constitutive equations in terms of $\boldsymbol{\tau}^e$, u and v:

$$\begin{aligned}&\hat{\boldsymbol{\tau}}^e + \lambda_1((\hat{\mathbf{U}}.\hat{\boldsymbol{\nabla}})\hat{\boldsymbol{\tau}}^e - (\hat{\boldsymbol{\nabla}}\hat{\mathbf{U}})^{\mathrm{T}}.\hat{\boldsymbol{\tau}}^e - \hat{\boldsymbol{\tau}}^e.(\hat{\boldsymbol{\nabla}}\hat{\mathbf{U}}))\\ &\quad - (\lambda_1 - \lambda_2)\hat{\eta}_0((\hat{\mathbf{U}}.\hat{\boldsymbol{\nabla}})\hat{\boldsymbol{\gamma}}_{(1)} - (\hat{\boldsymbol{\nabla}}\hat{\mathbf{U}})^{\mathrm{T}}.\hat{\boldsymbol{\gamma}}_{(1)} - \hat{\boldsymbol{\gamma}}_{(1)}.(\hat{\boldsymbol{\nabla}}\hat{\mathbf{U}})) = 0\end{aligned} \tag{7}$$

$$\hat{\boldsymbol{\tau}}^v = -\hat{\eta}_0(\hat{\boldsymbol{\nabla}}\hat{\mathbf{U}} + (\hat{\boldsymbol{\nabla}}\hat{\mathbf{U}})^{\mathrm{T}}) \tag{8}$$

3. GOVERNING DIFFERENTIAL EQUATIONS FOR 2-D STEADY POLYMER FLOW UTILIZING OLDROYD-B MODEL

For two-dimensional steady flow of Oldroyd-B fluid the governing differential equations consist of continuity, x and y momentum and Oldroyd-B constitutive equations (considering (6)), relating total stresses, strain rate tensor and fluid properties.

Copyright © 2006 John Wiley & Sons, Ltd.

3.1. Governing differential equations in velocities, pressure and total stresses

$$\hat{\nabla}.\hat{\mathbf{U}} = 0 \tag{9}$$

$$\hat{\rho}(\hat{\mathbf{U}}.\hat{\nabla})\hat{\mathbf{U}} + \hat{\nabla}.\hat{p} + \hat{\nabla}.\hat{\boldsymbol{\tau}} = 0 \tag{10}$$

$$\hat{\boldsymbol{\tau}} + \lambda_1((\hat{\mathbf{U}}.\hat{\nabla})\hat{\boldsymbol{\tau}} - (\hat{\nabla}\hat{\mathbf{U}})^{\mathrm{T}}.\hat{\boldsymbol{\tau}} - \hat{\boldsymbol{\tau}}.(\hat{\nabla}\hat{\mathbf{U}})) + \hat{\eta}_0\hat{\boldsymbol{\gamma}}_{(1)}$$

$$+ \lambda_2\hat{\eta}_0((\hat{\mathbf{U}}.\hat{\nabla})\hat{\boldsymbol{\gamma}}_{(1)} - (\hat{\nabla}\hat{\mathbf{U}})^{\mathrm{T}}.\hat{\boldsymbol{\gamma}}_{(1)} - \hat{\boldsymbol{\gamma}}_{(1)}.(\hat{\nabla}\hat{\mathbf{U}})) = 0 \quad \forall \hat{x}, \hat{y} \in \Omega_{\hat{x},\hat{y}} \tag{11}$$

Dimensionless form of these equations can be obtained by choosing following dimensionless variables: $x = \hat{x}/L_0$, $y = \hat{y}/L_0$, $\mathbf{U} = \hat{\mathbf{U}}/U_0$, $\boldsymbol{\tau} = \hat{\boldsymbol{\tau}}/\tau_0$, $p = \hat{p}/\tau_0$, $\rho = \hat{\rho}/\rho_0$, $\eta = \hat{\eta}_0/\eta_0$ where L_0, U_0, ρ_0, η_0 and τ_0 are reference length, velocity, density, viscosity and stress, respectively. If we choose $\rho_0 = \hat{\rho}$, then $\rho = 1$ and we have the following:

$$\nabla.\mathbf{U} = \mathbf{0} \tag{12}$$

$$f_1(\mathbf{U}.\nabla)\mathbf{U} + \nabla.p + \nabla.\boldsymbol{\tau} = 0 \tag{13}$$

$$\boldsymbol{\tau} + De_1((\mathbf{U}.\nabla)\boldsymbol{\tau} - (\boldsymbol{\tau}.\nabla\mathbf{U})^{\mathrm{T}} - (\boldsymbol{\tau}.\nabla\mathbf{U})) + \eta f_2(\nabla\mathbf{U} + (\nabla\mathbf{U})^{\mathrm{T}})$$

$$+ De_2 f_2((\mathbf{U}.\nabla)\boldsymbol{\gamma}_{(1)} - (\nabla\mathbf{U})^{\mathrm{T}}.\boldsymbol{\gamma}_{(1)} - \boldsymbol{\gamma}_{(1)}.(\nabla\mathbf{U})) = 0 \tag{14}$$

where $\boldsymbol{\gamma}_{(1)} = (\nabla\mathbf{U} + (\nabla\mathbf{U})^{\mathrm{T}})$ and $f_1 = \rho_0 {U_0}^2/\tau_0$, $f_2 = \eta_0 U_0/(\tau_0 L_0)$, $De_1 = \lambda_1 U_0/L_0$ (Deborah number), $De_2 = \lambda_2 U_0/L_0$. If we choose $\tau_0 = \rho_0 U_0^2$ (reference stress based on characteristic kinetic energy), then $f_1 = 1, f_2 = 1/Re$ and if $\tau_0 = \eta_0 U_0/L_0$ (reference stress based on characteristic viscous stress), then $f_1 = Re, f_2 = 1$, where $Re = \rho_0 U_0 L_0/\eta_0$ (Reynolds number).

3.2. GDEs in terms of velocities, pressure and elastic stresses

In this set of GDEs, we have continuity, momentum equations in which $\hat{\boldsymbol{\tau}} = \hat{\boldsymbol{\tau}}^e + \hat{\boldsymbol{\tau}}^v$ with $\hat{\boldsymbol{\tau}}^v = -\hat{\eta}_0(\hat{\nabla}.\hat{\mathbf{U}} + (\hat{\nabla}.\hat{\mathbf{U}})^{\mathrm{T}})$ is substituted in the momentum equations. The resulting equations are given in the following:

$$\hat{\nabla}.\hat{\mathbf{U}} = 0 \tag{15}$$

$$\hat{\rho}(\hat{\mathbf{U}}.\hat{\nabla})\hat{\mathbf{U}} + \hat{\nabla}\hat{p} + \hat{\nabla}.\hat{\boldsymbol{\tau}}^e - \hat{\eta}_0\hat{\nabla}.(\hat{\nabla}.\hat{\mathbf{U}} + (\hat{\nabla}.\hat{\mathbf{U}})^{\mathrm{T}}) = 0 \tag{16}$$

$$\hat{\boldsymbol{\tau}}^e + \lambda_1((\hat{\mathbf{U}}.\hat{\nabla})\hat{\boldsymbol{\tau}}^e - (\hat{\nabla}\hat{\mathbf{U}}).\hat{\boldsymbol{\tau}}^e - \hat{\boldsymbol{\tau}}^e.(\hat{\nabla}\hat{\mathbf{U}}))$$

$$- (\lambda_1 - \lambda_2)\hat{\eta}_0((\hat{\mathbf{U}}.\hat{\nabla})\hat{\boldsymbol{\gamma}}_{(1)} - (\hat{\nabla}.\hat{\mathbf{U}})^{\mathrm{T}}.\hat{\boldsymbol{\gamma}}_{(1)} - \hat{\boldsymbol{\gamma}}_{(1)}.(\hat{\nabla}\hat{\mathbf{U}})) = 0 \tag{17}$$

These equations can be non-dimensionalized using the same approach as in Section 3.1.

Copyright © 2006 John Wiley & Sons, Ltd.

Remarks

(1) GDEs in (12)–(14) or (15)–(17) are a system of non-linear partial differential equations in u, v, p, $\boldsymbol{\tau}$ or $\boldsymbol{\tau}^e$ in which only first-order derivatives of p, $\boldsymbol{\tau}$ or $\boldsymbol{\tau}^e$ appear while the equations contain upto second-order derivatives of u and v w.r.t. x and y.

(2) If we assume that the theoretical solutions of (12)–(14) or (15)–(17) (though may not be obtainable) are analytic, i.e. u, v, p and $\boldsymbol{\tau}$ or $\boldsymbol{\tau}^e$ are analytic, then u, v, p and $\boldsymbol{\tau}$ or $\boldsymbol{\tau}^e$ are polynomial of infinite degree in x and y. Such solutions are of class $C^\infty(\Omega_{xy})$ in which derivatives of all orders exist, are continuous and are square integrable (due to analytic nature of solution). This feature of the theoretical solution is significant and permits us to design a precise mathematical and computational framework to address their numerical simulations. Numerical simulations of singular BVP have also been addressed by Surana *et al.* [31] using the same mathematical and computational framework as utilized here.

4. MATHEMATICAL FRAMEWORK AND APPROXIMATION SPACES $H^k(\bar{\Omega}^{\mathrm{T}}_{xy})$ AND $H^{k,p}(\bar{\Omega}^e_{xy})$

The mathematical and computational framework based on h, p, k; the characteristic length, degree of local approximation and the order of the approximation space as independent computational parameters and variationally consistent integral forms [25–27] is utilized for numerical simulation of two-dimensional flows of Oldroyd-B fluids. This framework permits higher order global differentiability approximations necessitated by the theoretical solutions when they are analytic. The order of the space k controls the global differentiability of approximations.

Let φ be the dependent variable and let $\bar{\Omega}^{\mathrm{T}}_{xy} = \bigcup_e \bar{\Omega}^e_{xy}$ be a discretization of $\bar{\Omega}_{xy}$ containing 'M' subdomains in which $\bar{\Omega}^e_{xy}$ is a subdomain (element) 'e'. Let φ^e_h be local approximation of φ over $\bar{\Omega}^e_{xy}$, then φ_h, the global approximation of φ over $\bar{\Omega}^{\mathrm{T}}_{xy}$ is given by

$$\varphi_h = \bigcup_e \varphi^e_h$$

We define approximation spaces or scalar product spaces for global approximation φ_h and local approximation φ^e_h for a dependent variable φ. Let $H^k(\bar{\Omega}^{\mathrm{T}}_{xy})$ be scalar product space of order k containing φ_h of class $c^{k-1}(\bar{\Omega}^{\mathrm{T}}_{xy})$. Since $\varphi_h = \bigcup_e \varphi^e_h$, we define scalar product space $H^{k,p}(\bar{\Omega}^e_{xy})$ to be the approximation space for the local approximations φ^e_h over $\bar{\Omega}^e$ in which k is the order of the space and p is the degree of local approximations. This local approximation space contains functions of class $c^{k-1}(\bar{\Omega}^e_{xy})$ and degree p. In the present work, we use algebraic monomials or polynomials for constructing local approximations functions [32].

5. GALERKIN METHOD AND GALERKIN METHOD WITH WEAK FORM

Since the differential operator in (12)–(14) or (15)–(17) is non-linear both Galerkin method and Galerkin method with weak form are variationally inconsistent, i.e. the resulting finite

Copyright © 2006 John Wiley & Sons, Ltd.

element processes yield non-symmetric coefficient matrices which may have partial or completely complex basis and hence the computational processes may produce spurious solutions or may even totally degenerate. A significant point to note here is that variational consistency of these integral forms resulting from Galerkin or Galerkin method with weak form cannot be restored through any mathematically justifiable means and hence the resulting numerical processes may have the possibility of producing spurious solutions or may even totally degenerate [25–27, 33, 34]. Hence, these methods cannot be viewed as viable and reliable computational strategies.

6. LEAST SQUARES PROCESSES IN Ω_{xy} (NO DISCRETIZATION)

In contrast to Galerkin method or Galerkin method with weak form, least square processes are variationally consistent for non-linear differential operators and hence yield coefficient matrices that are symmetric and positive definite and that always have a real basis and thus are naturally free of spuriousness [33, 34]. First, we present details of the least squares process in Ω_{xy} (no discretization) and then least square element processes in $H^{k,p}(\bar{\Omega}^e)$ spaces followed by a discussion of minimally conforming spaces for both form of the governing differential equations, i.e. (12)–(14) and (15)–(17) and reasons for the need for higher order spaces than minimally conforming. Let

$$[\varphi_h]^{\mathrm{T}} = [u_h, v_h, p_h, (\tau_{xx})_h, (\tau_{xy})_h, (\tau_{yy})_h] \tag{18}$$

or

$$[\varphi_h]^{\mathrm{T}} = [u_h, v_h, p_h, (\tau^e_{xx})_h, (\tau^e_{xy})_h, (\tau^e_{yy})_h] \tag{19}$$

be the global approximations of velocities, pressure and stresses for (12)–(14) and (15)–(17). For subsequent details, consider GDEs (12)–(14). Upon substituting these approximations in the governing differential equations (12)–(14) we obtain residual equations for Ω_{xy},

$$E_1 = \frac{\partial u_h}{\partial x} + \frac{\partial v_h}{\partial y} \tag{20}$$

$$E_2 = f_1\left(u_h\frac{\partial u_h}{\partial x} + v_h\frac{\partial u_h}{\partial y}\right) + \frac{\partial p_h}{\partial x} + \frac{\partial (\tau_{xx})_h}{\partial x} + \frac{\partial (\tau_{xy})_h}{\partial y} \tag{21}$$

$$E_3 = f_1\left(u_h\frac{\partial v_h}{\partial x} + v_h\frac{\partial v_h}{\partial y}\right) + \frac{\partial p_h}{\partial y} + \frac{\partial (\tau_{xy})_h}{\partial x} + \frac{\partial (\tau_{yy})_h}{\partial y} \tag{22}$$

$$E_4 = (\tau_{xx})_h + De_1\left(u_h\frac{\partial (\tau_{xx})_h}{\partial x} + v_h\frac{\partial (\tau_{xx})_h}{\partial y} - 2\frac{\partial u_h}{\partial x}(\tau_{xx})_h - 2\frac{\partial u_h}{\partial y}(\tau_{xy})_h\right) + 2\eta f_2\frac{\partial u_h}{\partial x}$$

$$+ De_2 f_2\left(2u_h\frac{\partial^2 u_h}{\partial x^2} + 2v_h\frac{\partial^2 u_h}{\partial y \partial x} - 4\left(\frac{\partial u_h}{\partial x}\right)^2 - 2\frac{\partial u_h}{\partial y}\left(\frac{\partial u_h}{\partial y} + \frac{\partial v_h}{\partial x}\right)\right) \tag{23}$$

Copyright © 2006 John Wiley & Sons, Ltd.

$$E_5 = (\tau_{xy})_h + De_1\left(u_h\frac{\partial(\tau_{xy})_h}{\partial x} + v_h\frac{\partial(\tau_{xy})_h}{\partial y} - \frac{\partial v_h}{\partial x}(\tau_{xx})_h - \frac{\partial u_h}{\partial y}(\tau_{yy})_h\right)$$
$$- De_1\left(\left(\frac{\partial u_h}{\partial x} + \frac{\partial v_h}{\partial y}\right)(\tau_{xy})_h\right) + \eta f_2\left(\frac{\partial u_h}{\partial y} + \frac{\partial v_h}{\partial x}\right)$$
$$- De_2 f_2\left(u_h\left(\frac{\partial^2 u_h}{\partial y\partial x} + \frac{\partial^2 v_h}{\partial x^2}\right) + v_h\left(\frac{\partial^2 u_h}{\partial y^2} + \frac{\partial^2 v_h}{\partial y\partial x}\right) - 2\frac{\partial u_h}{\partial y}\frac{\partial v_h}{\partial y}\right)$$
$$- De_2 f_2\left(2\frac{\partial u_h}{\partial x}\frac{\partial v_h}{\partial x} + \left(\frac{\partial u_h}{\partial x} + \frac{\partial v_h}{\partial y}\right)\left(\frac{\partial u_h}{\partial y} + \frac{\partial v_h}{\partial x}\right)\right) \tag{24}$$

$$E_6 = (\tau_{yy})_h + De_1\left(u_h\frac{\partial(\tau_{yy})_h}{\partial x} + v_h\frac{\partial(\tau_{yy})_h}{\partial y} - 2\frac{\partial v_h}{\partial y}(\tau_{yy})_h - 2\frac{\partial v_h}{\partial x}(\tau_{xy})_h\right) + 2\eta f_2\frac{\partial v_h}{\partial y}$$
$$+ De_2 f_2\left(2u_h\frac{\partial^2 v_h}{\partial y\partial x} + 2v_h\frac{\partial^2 v_h}{\partial y^2} - 2\frac{\partial v_h}{\partial x}\left(\frac{\partial u_h}{\partial y} + \frac{\partial v_h}{\partial x}\right) - 4\left(\frac{\partial v_h}{\partial y}\right)^2\right) \tag{25}$$

In least squares process, we begin with the construction of a functional I [35–37] using residual equations (20)–(25),

(i) *Existence of functional I*:

$$I(\varphi_h) = \sum_{i=1}^{6}(E_i, E_i) = \sum_{i=1}^{6}\int_{\Omega_{xy}}(E_i)^2\,\mathrm{d}\Omega \tag{26}$$

Clearly I describes a convex manifold and furthermore, the convexity of the manifold is independent of the differential operator.

(ii) *Necessary condition*: Necessary condition is obtained by setting $\delta I(\varphi_h) = 0$ (provided $I(\varphi_h)$ is differentiable in φ_h),

$$\delta I(\varphi_h) = \sum_{i=1}^{6}(E_i, \delta E_i) = \{g(\varphi_h)\} = 0 \tag{27}$$

(iii) *Sufficient conditions* (*extremum principle*): Second variation of $I(\varphi_h)$, i.e. $\delta^2 I(\varphi_h)$ (provided $I(\varphi_h)$ is differentiable twice in φ_h) provides sufficient conditions or extremum principle. Based on References [25–27], we can write,

$$\delta^2 I(\varphi_h) \cong \sum_{i=1}^{6}(\delta E_i, \delta E_i) > 0 \tag{28}$$

(i)–(iii) clearly establish that the least squares process is variationally consistent.

(iv) We now must find a solution φ_h that satisfies (27). However, since $\{g(\varphi_h)\}$ is a non-linear function of φ_h due to the fact that the GDEs are non-linear, hence, we must find φ_h iteratively. Following Surana *et al.* [25–27], if φ_h^0 is a starting or assumed solution, then $\{g(\varphi_h)\}$ can be expanded in Taylor series about φ_h^0, and limiting to

Copyright © 2006 John Wiley & Sons, Ltd.

first-order approximation (Newton's linear method) we obtain the following:

$$\varphi_h = \varphi_h^0 + \alpha \Delta\varphi_h \tag{29}$$

$$\Delta\varphi_h = -[\delta^2 I(\varphi_h)]^{-1}_{\varphi_h^0} \{g(\varphi_h)\}_{\varphi_h^0} \tag{30}$$

in which α is a constant generally between 0 and 2 determined such that $I(\varphi_h) \leqslant I(\varphi_h^0)$. This procedure is termed Newton's method with line search. we already have expression for $E_i,\ i=1,2,\ldots,6$ in (20)–(25) and approximation φ_h involving unknown constant and basis functions. All that we need now are expressions for $\delta E_i,\ i=1,2,\ldots,6$, which can be easily obtained using $E_i,\ i=1,2,\ldots,6$ and differentiating them with respect to the constants used in the approximation φ_h.

Remarks

(1) First, we note that the coefficient matrix in $\Delta\varphi_h$ calculation is given by $\delta^2 I(\varphi_h)$ in (28). Since $\delta^2 I(\varphi_h) > 0$, for any choice of computational and physical parameters, the coefficient matrix is always positive definite and hence always has a real basis and thus the resulting computational process will always be pollution free.
(2) Equation (28) assures that a solution φ_h minimizes $I(\varphi_h)$ in (26).
(3) Minima of $I(\varphi_h)$ is zero, which is only possible when $E_i \equiv 0$ in Ω_{xy} in the point-wise sense, i.e. a minima of $I(\varphi_h)$ in (i)–(iv) also satisfies governing differential equations in the point-wise sense and hence is a solution of the boundary value problem also.
(4) Since approximation φ_h is global over Ω_{xy} (no discretization), there are no issues of global differentiability of φ_h.

7. LEAST SQUARES FINITE ELEMENT PROCESSES

Let $\bar{\Omega}^{\mathrm{T}}_{xy} = \bigcup_e^M \bar{\Omega}^e_{xy}$ be a discretization of $\bar{\Omega}_{xy}$ containing 'M' subdomains in which $\bar{\Omega}^e_{xy}$ is a subdomain (element) 'e' and let φ_h^e be local approximation of φ over $\bar{\Omega}^e_{xy}$, then φ_h, global approximation of φ over $\bar{\Omega}^{\mathrm{T}}_{xy}$ is given by

$$\varphi_h = \bigcup_e^M \varphi_h^e \tag{31}$$

The details presented in Section 6 for least squares processes over Ω_{xy} can be recast for the discretization $\bar{\Omega}^{\mathrm{T}}_{xy}$.

(i) *Existence of functional $I(\varphi_h)$ for $\bar{\Omega}^{\mathrm{T}}_{xy}$*:

$$I(\varphi_h) = \sum_{e=1}^{M}\sum_{i=1}^{6} (E_i^e, E_i^e) = \sum_{e=1}^{M}\sum_{i=1}^{6} \int_{\Omega^e_{xy}} (E_i)^2 \, \mathrm{d}\Omega \tag{32}$$

in which E_i^e are the element residual quantities obtained from (12)–(14) or (15)–(17) by substituting φ_h^e.

Copyright © 2006 John Wiley & Sons, Ltd.

(ii) *Necessary condition*: These are obtained by setting $\delta I(\varphi_h) = 0$, provided $I(\varphi_h)$ is differentiable in φ_h,

$$\delta I(\varphi_h) = \sum_{e=1}^{M} \sum_{i=1}^{6} (E_i^e, \delta E_i^e) = \sum_{e=1}^{M} \{g^e(\varphi_h^e)\} = \{g(\varphi_h)\} = 0 \tag{33}$$

(iii) *Sufficient conditions* (*extremum principle*): If $I(\varphi_h)$ is differentiable twice in φ_h, then $\delta^2 I(\varphi_h)$ provides the extremum principle, and based on Surana *et al.* [25–27] we have,

$$\delta^2 I(\varphi_h) \cong \sum_{e=1}^{M} \sum_{i=1}^{6} (\delta E_i^e, \delta E_i^e) = \sum_{e=1}^{M} \sum_{i=1}^{6} \delta^2 I^e(\varphi_h^e) \tag{34}$$

(iv) Newtons method with line search becomes,

$$\varphi_h = \varphi_h^o + \alpha \Delta \varphi_h \tag{35}$$

$$\Delta \varphi_h = -[\delta^2 I(\varphi_h)]^{-1}_{\varphi_h^0} \{g(\varphi_h)\}_{\varphi_h^0} \tag{36}$$

Remarks

(1) Variational consistency of this least squares finite element process inherently stems from the variational consistency of least squares process over Ω_{xy} presented in Section 6. Hence, the remarks presented in Section 6 hold here as well.
(2) The nature of local approximation φ_h^e is crucial, so that we can establish the Hilbert spaces containing basis functions for local approximations φ_h^e.

7.1. Local approximation spaces for least squares finite element process for GDEs (12)–(14) or (15)–(17)

In this section, we consider local approximation φ_h^e for governing differential equations (12)–(14). These are a set of non-linear partial differential equations in u, v, p and $\boldsymbol{\tau}$ in which only first-order derivatives of p and $\boldsymbol{\tau}$ appear but the highest order of derivatives of u and v is two. For the integrands in the LSP to be continuous the approximations p_h and $\boldsymbol{\tau}_h$ must atleast be of class $C^1(\bar{\Omega}^{\mathrm{T}}_{xy})$ and u_h and v_h must be atleast of class $C^2(\bar{\Omega}^{\mathrm{T}}_{xy})$ and since the global approximation φ_h is given by (31), it follows that in φ_h^e, p_h^e and $(\boldsymbol{\tau}_h^e)^e$ must also be of class $C^1(\bar{\Omega}^e_{xy})$ and u_h^e, v_h^e must be of class $C^2(\bar{\Omega}^e_{xy})$, i.e. $H^{2,p}(\bar{\Omega}^e_{xy})$ is the minimally conforming spaces for p_h^e and $(\boldsymbol{\tau}_h)^e$ whereas $H^{3,p}(\bar{\Omega}^e_{xy})$ is the minimally conforming spaces for u_h^e and v_h^e. The need for higher order spaces is rather obvious if φ_h is to approach φ in terms of global differentiability in the point-wise sense. We remark that p^e and $(\boldsymbol{\tau}_h)^e$ of class $C^2(\bar{\Omega}^e_{xy})$ are admissible in the integrands too. Thus, it perhaps may be convenient to consider $H^{3,p}(\bar{\Omega}^e_{xy})$ as the minimally conforming space for φ_h^e instead of different order spaces for p_h^e, $(\boldsymbol{\tau}_h)^e$ and u_h^e, v_h^e. Hence, we have the following:

$$\varphi_h \in H^k(\bar{\Omega}^{\mathrm{T}}_{xy}), \quad k \geqslant 3 \tag{37}$$

$$\varphi_h^e \in H^{k,p}(\bar{\Omega}^{\mathrm{T}}_{xy}), \quad k \geqslant 3 \tag{38}$$

In which $k = 3$ is the minimally conforming space for all variables. Same arguments hold for GDEs in u, v, p and $\boldsymbol{\tau}^e$ variables.

Copyright © 2006 John Wiley & Sons, Ltd.

7.2. Local approximation φ_h^e over $(\bar{\Omega}_{xy}^e)$

Hence for both forms of the GDEs discussed here, we can write the following:

$$\varphi_h^e \in V_h(\bar{\Omega}_{xy}^e) = H^{k,p}(\bar{\Omega}_{xy}^e) \tag{39}$$

In which we define,

$$V_h(\bar{\Omega}_{xy}^e) = H^{k,p}(\bar{\Omega}_{xy}^e) = \{w : w|_{\bar{\Omega}_{xy}^e} \in C^{k-1}, w|_{\bar{\Omega}_{xy}^e} \in P^p \ \forall \bar{\Omega}_{xy}^e \in \bar{\Omega}_{xy}^{\mathrm{T}}\} \tag{40}$$

$\varphi_h^e \in V_h(\bar{\Omega}_{xy}^e)$ can be interpreted using,

$$\varphi_h^e \in [N^{k-1,p}(x,y)]\{\delta^e\} \quad \forall (x,y) \in \bar{\Omega}_{xy}^e \tag{41}$$

In which $\{\delta^e\}$ are the nodal degrees of freedom for all variables for a subdomain $\bar{\Omega}_{xy}^e$. If the basis functions $N^{k-1,p}(x,y) \in H^{k,p}(\bar{\Omega}_{xy}^e)$ then obviously $\varphi_h^e \in H^{k,p}(\bar{\Omega}_{xy}^e)$.

8. NUMERICAL STUDIES

In this section, we represent a number of numerical studies using: (i) fully developed flow between parallel plates and (ii) a lid driven square cavity as model problems. Numerical studies are designed to demonstrate many features of the approach presented in this paper some of which are outlined in the following:

(1) For a given order of approximation space, i.e. k and a fixed discretization (h), it is possible to obtain a converging sequence of solutions, that is with progressively increasing p-levels, the sequence of solutions has a limit point.
(2) The process in (1) is carried out for progressively increasing order of the approximation space and thus obtaining a sequence of limit points that is shown to converge with increasing k. Hence, we obtain a limit point of the sequence of limit points that is independent of p and k.
(3) The process in (1) and (2) is repeated for as many progressively refined uniform (or quasi-uniform) discretizations as needed until the limit points in (2) for two successive discretizations are in close agreement and thus yielding a solution that is independent of h, p and k.
(4) Oldroyd-B model is a constitutive model designed for dilute polymer solutions with some elasticity but essentially solvent, i.e. viscous dominated behaviour. This model like UCMM has only one elastic parameter λ_1, the relaxation time. The retardation time, λ_2 allows one to tune the model to either closer to Newtonian or Maxwell or any place in between. It is significant to keep in mind that the mechanism of elasticity in UCMM and Oldroyd-B model is identical, i.e. Oldroyd-B model like UCMM fails to incorporate the correct physics of two-dimensional elasticity which requires at least a minimum of two elastic constants. Another significant point to note is that from the published experimental work dealing with dilute polymer solutions [38], we note that (Figure 1) Oldroyd-B model has an upper limit of $\hat{\dot{\gamma}} = 3$ (for M1 fluid used here) beyond which the first normal stress difference versus $\hat{\dot{\gamma}}$ predicted by the model begins to deviate

Copyright © 2006 John Wiley & Sons, Ltd.

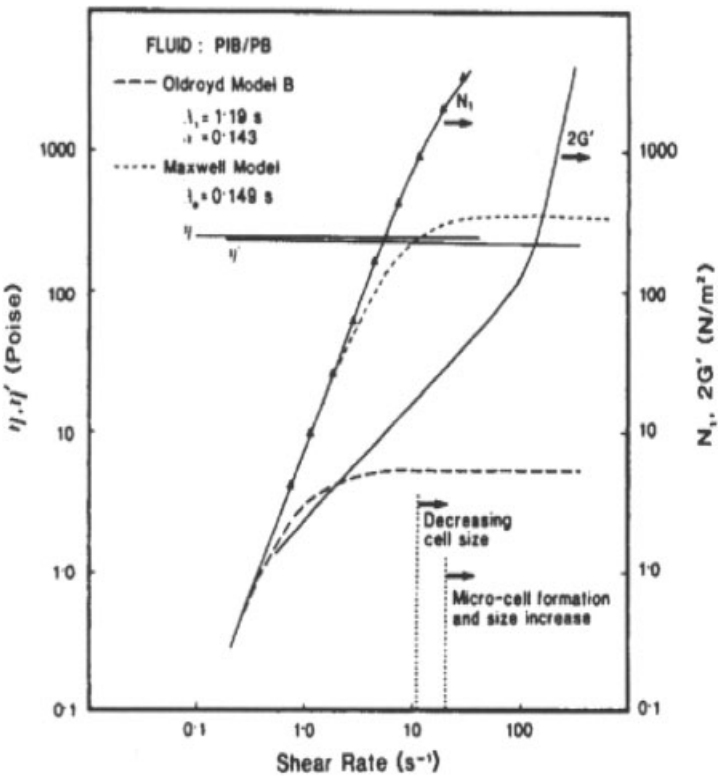

Figure 1. First normal stress difference and storage modulus for the polyisobutylene-polybutene solution used in the flow visualization experiments—comparison between experiment and prediction with the Maxwell and Oldroyd B model [38].

significantly from the experimental data. This does not mean that for $\hat{\dot{\gamma}}$ beyond 3 one would observe the failure of numerical simulations. All it says is that beyond $\hat{\dot{\gamma}} = 3$, the numerical simulations are no longer in agreement with the experiments.

8.1. *Fully developed flow between parallel plates*

For fully developed flow between parallel plates the GDEs have a theoretical solution given by

$$\tau_{xy}^{p} = -\frac{n_p}{(n_p + n_s)}\left(\frac{\partial p}{\partial x}\right) y$$

$$\tau_{xy}^{s} = -\frac{n_s}{(n_p + n_s)}\left(\frac{\partial p}{\partial x}\right) y$$

$$\tau_{xx}^{e} = -\frac{2De\eta_p}{(\eta_p + \eta_s)^2}\left(\frac{\partial p}{\partial x}\right)^2 y^2$$

Copyright © 2006 John Wiley & Sons, Ltd.

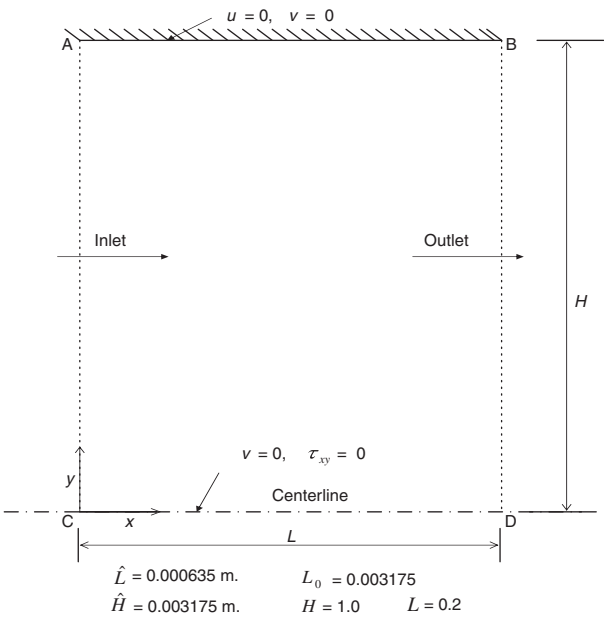

Figure 2. Schematic of computational domain for fully developed flow between parallel plates.

Figure 2 shows a schematic of the computational domain and the boundary conditions. We choose M1 fluid [39] with the following properties: $\hat{\rho} = 868\,\text{kg/m}^3$, $\hat{\eta}_s = 2.7\,\text{Pa s}$, $\hat{\eta}_p = 0.3\,\text{Pa s}$, $\lambda_1 = 0.1\,\text{s}$, $\hat{\eta} = \hat{\eta}_s + \hat{\eta}_p = 3\,\text{Pa s}$.

If we choose reference viscosity $\eta_0 = \hat{\eta}$, then $\eta = 1$ and $\eta_s = \hat{\eta}_s/\eta_0 = 0.9$, $\eta_p = \hat{\eta}_p/\eta_0 = 0.1$ and the dimensionless parameters, Reynolds number and Deborah number, are given by $Re = (\rho_0 L_0/\eta_0)u_0 = 0.918633u_0$, $De = (\lambda_1/L_0)u_0 = 31.4960629u_0$.

A five element uniform discretizations is considered in the y-direction for all numerical studies shown in Figure 4. Flow rates are uniformly increased by choosing $u_0 = 0.1$, 1.0, 5.0 and 10.0 corresponding to $De = 3.1496$, 31.496, 157.48 and 314.96, respectively. Numerical studies are presented for $\lambda_2 = \lambda_1/2 = 0.05$. The purpose of presenting numerical studies for higher De for which the strain rates are well beyond the range of validity of Oldroyd-B model is to demonstrate: (1) that for highly specialized flows such as this model problem in which the flow in unidirectional, the Oldroyd-B model (which is primarily 1-D model) may not result in the failure of the computations; (2) that the computational process is quite robust regardless of the unrealistic behaviour of Oldroyd-B model. The purpose of these numerical studies is not to validate the computational process even though one could. In the computational approach presented here when least squares functional I approaches zero, we indeed have a numerical solution that satisfies the GDE in the point-wise sense in the whole domain. This is the major strength and significant feature of the computational approach presented here. For each flow rate solutions of class C^1 are computed by progressively increasing p-levels ($p_\xi = p_\eta = p$) uniformly for all elements of the discretization until the numerical solutions from two successive p-levels do not show any appreciable change. Figure 4 shows graphs of $\hat{u}$, $\hat{\tau}^e_{xx}$, $\hat{\tau}^v_{xy}$ and $\hat{\dot{\gamma}}$ versus y at convergence ($p = 5$). In the following we make some remarks

Copyright © 2006 John Wiley & Sons, Ltd.

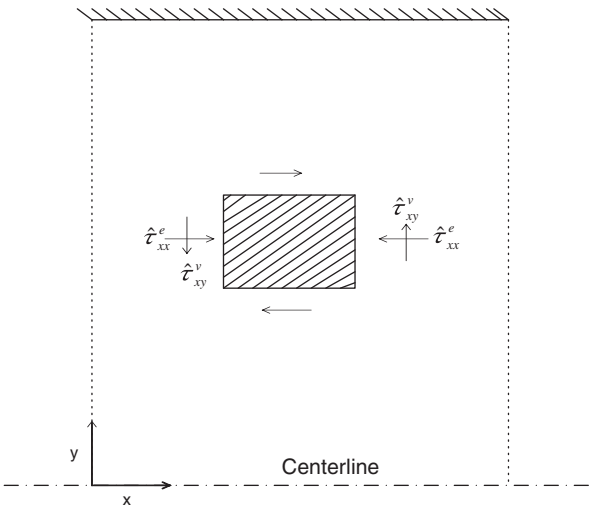

Figure 3. Equilibrium of an elementary fluid volume for fully developed flow between parallel plates.

and discuss some important aspects of the flow physics and the constitutive model behaviour.

(1) From the results shown in Figure 4 we observe that numerical computations are successful well beyond the range of validity of $\hat{\dot{\gamma}}$. Results are presented for De as high as 314.96 (and beyond, not shown) but the first normal stress difference is not in agreement with experiments beyond $\hat{\dot{\gamma}} = 3$.

(2) As discussed earlier, the Oldroyd-B model lacks correct physics of two-dimensional elasticity, i.e. the model is incapable of predicting the change in the direction normal to the applied stress or disturbance. This is clearly evident by $\hat{\tau}^{e}_{yy} = 0$ even though $\hat{\tau}^{e}_{xx} \neq 0$.

(3) One might wonder that inspite of such basic shortcoming of the correct physics of elasticity (as described in (2)), the Oldroyd-B model produces converged solutions for this simple flow situation. The answer to this question is rather simple if one considers the equilibrium of an elementary fluid volume. In this case, the only non-zero stresses generated from the numerical solution of the GDEs are: $\hat{\tau}^{v}_{xy}$ and $\hat{\tau}^{e}_{xx}$, which when acting on an elementary fluid volume maintain equilibrium of the fluid volume regardless of the flow rate and hence for any value of $\hat{\dot{\gamma}}$ and De (Figure 3). Since the model has no mechanism for $\hat{\tau}^{e}_{yy}$ it produces $\hat{\tau}^{e}_{yy} = 0$ which in this case can be tolerated without disturbing the equilibrium of the fluid volume and hence the reason for success of the numerical simulations for any value of $\hat{\dot{\gamma}}$.

(4) It is well known that $\hat{\tau}^{e}_{yy} = 0$ is non-physical and hence the results from the simulations for all $De \neq 0$ are non-physical. However, one could perhaps rationalize that at very low $\hat{\dot{\gamma}}$, $\hat{\tau}^{e}_{yy}$ is small compared to $\hat{\tau}^{e}_{xx}$ and hence perhaps the results for first normal stress difference are not in significant error and thus could be tolerated and hence the reason for accepting Oldroyd-B model results for low values of $\hat{\dot{\gamma}}$. But we know that $\hat{\tau}^{e}_{yy} \neq 0$ if $De \neq 0$ and hence Oldroyd-B model results for dilute polymer solutions are always non-physical and are in error.

Copyright © 2006 John Wiley & Sons, Ltd.

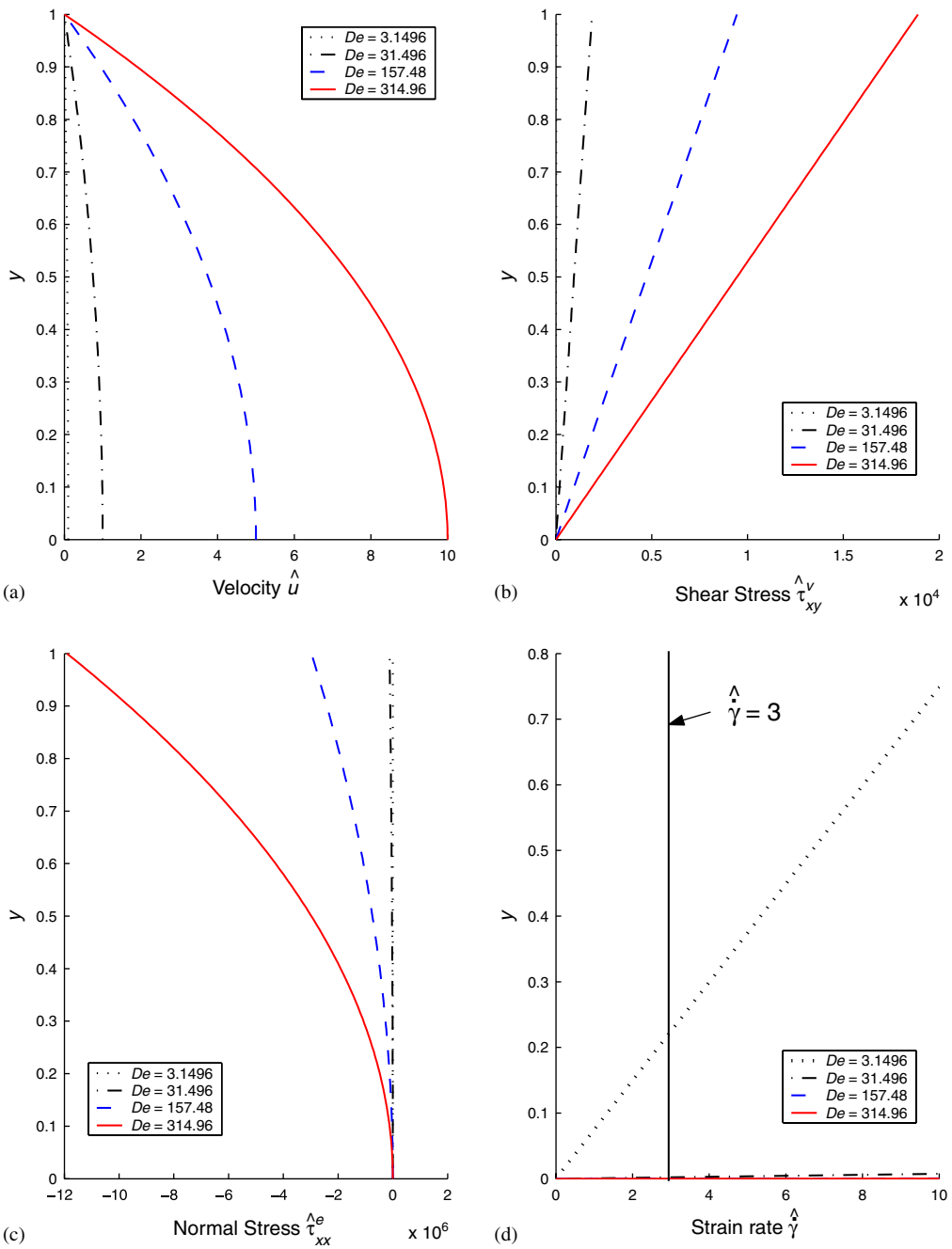

Figure 4. Fully developed flow: solutions of class C^1, $p = 5, \lambda_2 = 0.05$: (a) velocity $\hat{u}$ versus y; (b) shear stress $\hat{\tau}^v_{xy}$ versus y; (c) normal stress $\hat{\tau}^e_{xx}$ versus y; and (d) strain rate $\hat{\dot{\gamma}}$ versus y.

Copyright © 2006 John Wiley & Sons, Ltd.

(5) Lastly, we want to summarize that for this model problem numerical simulations are: (i) possible for any $\hat{\dot{\gamma}}$; (ii) possible because $\hat{\tau}^e_{yy} = 0$ does not disturb the equilibrium of the elementary fluid volume; (iii) are erroneous for all values of $De \neq 0$ due to the fact that based on the physics of two-dimensional elasticity $\hat{\tau}^e_{yy} \neq 0$ for all $De \neq 0$ but the model produces $\hat{\tau}^e_{yy} = 0$ for all $De \neq 0$.
(6) As additional information, Figure 5 shows graphs of first normal stress difference versus $\hat{\dot{\gamma}}$ at $y = 0.25$, 0.5, 0.75 and 1.0.
(7) The studies reported here are for $\lambda_2 = 0.05$ only. Similar behaviour is observed for $0 < \lambda_2 < \lambda_1$.

8.2. *Lid driven square cavity*

In this study we consider a lid driven square cavity as a model problem. Figure 6 shows a schematic of the cavity, idealization of the cavity for computations and four different discretizations:

Mesh M1: 36 element discretization ($h_d = 0.1$)
Mesh M2: 100 element discretization ($h_d = 0.1$)
Mesh M3: 49 element discretization ($h_d = 0.05$)
Mesh M4: 400 element discretization ($h_d = 0.05$)

We note that the points A and B where the stationary cavity walls meet the moving lid represent locations where description of velocity u is non-unique. The mathematical idealization proposed in Figure 6(b), in which u changes from zero at points A and B to one over a length h_d in a continuous and differentiable manner is designed to approach the true physics at A and B in the limiting process. When the distribution of u over h_d is of class C^k, then in the limit $h_d \to 0$ and $k \to \infty$ we indeed recover the true physics at points A and B, hence the motivation for the idealization shown in Figure 6(b). This representation of the velocity field along the lid makes u analytic. This is helpful in computations as the generalized solutions of non-linear singular BVP may be non-unique. It is demonstrated that with the choices of h_d used here the local behaviour at points A and B remains isolated in a very small neighbourhood around points A and B without disturbing rest of the flow field in the cavity. The singular behaviour at points A and B can only be approached as a limiting case as shown here.

We make remarks regarding the four meshes (M1, M2, M3 and M4). In mesh M1, a quasi-uniform mesh, $h_d = 0.1$. Mesh M2 also has $h_d = 0.1$ but has much more refined grid compared to mesh M1. These meshes would serve to show the mesh independence of the solution for $h_d = 0.1$. Meshes M3 and M4 with $h_d = 0.05$ are designed similar to meshes M1 and M2 and would serve to show the mesh independence of the solution for $h_d = 0.05$. We consider M1 fluid [38] with the following properties:

$$\hat{\rho} = 868\,\text{kg/m}^3, \quad \hat{\eta}_s = 2.7\,\text{Pa s}, \quad \hat{\eta}_p = 0.3\,\text{Pa s}, \quad \lambda_1 = 0.1\,\text{s}, \quad \hat{\eta} = \hat{\eta}_s + \hat{\eta}_p = 3\,\text{Pa s}, \quad \lambda_2 = 0.5$$

If we choose reference viscosity $\eta_0 = \hat{\eta}$, then $\eta = 1$ and $\eta_s = \hat{\eta}_s/\eta_0 = 0.9$, $\eta_p = \hat{\eta}_p/\eta_0 = 0.1$ and the dimensionless parameters, Reynolds number and Deborah number are given by $Re = (\rho_0 L_0/\eta_0)u_0$, $De = (\lambda_1/L_0)u_0$. Numerical simulations are considered for: $De = 0.2$, $u_0 = 0.2$, lid velocity $\hat{u}_l = 0.2\,\text{m/s}$ and $De = 0.4$, $u_0 = 0.4$, lid velocity $\hat{u}_l = 0.4\,\text{m/s}$ for all four meshes described above. We consider $\lambda_2 = 0.05$ for all numerical studies unless stated otherwise.

Copyright © 2006 John Wiley & Sons, Ltd.

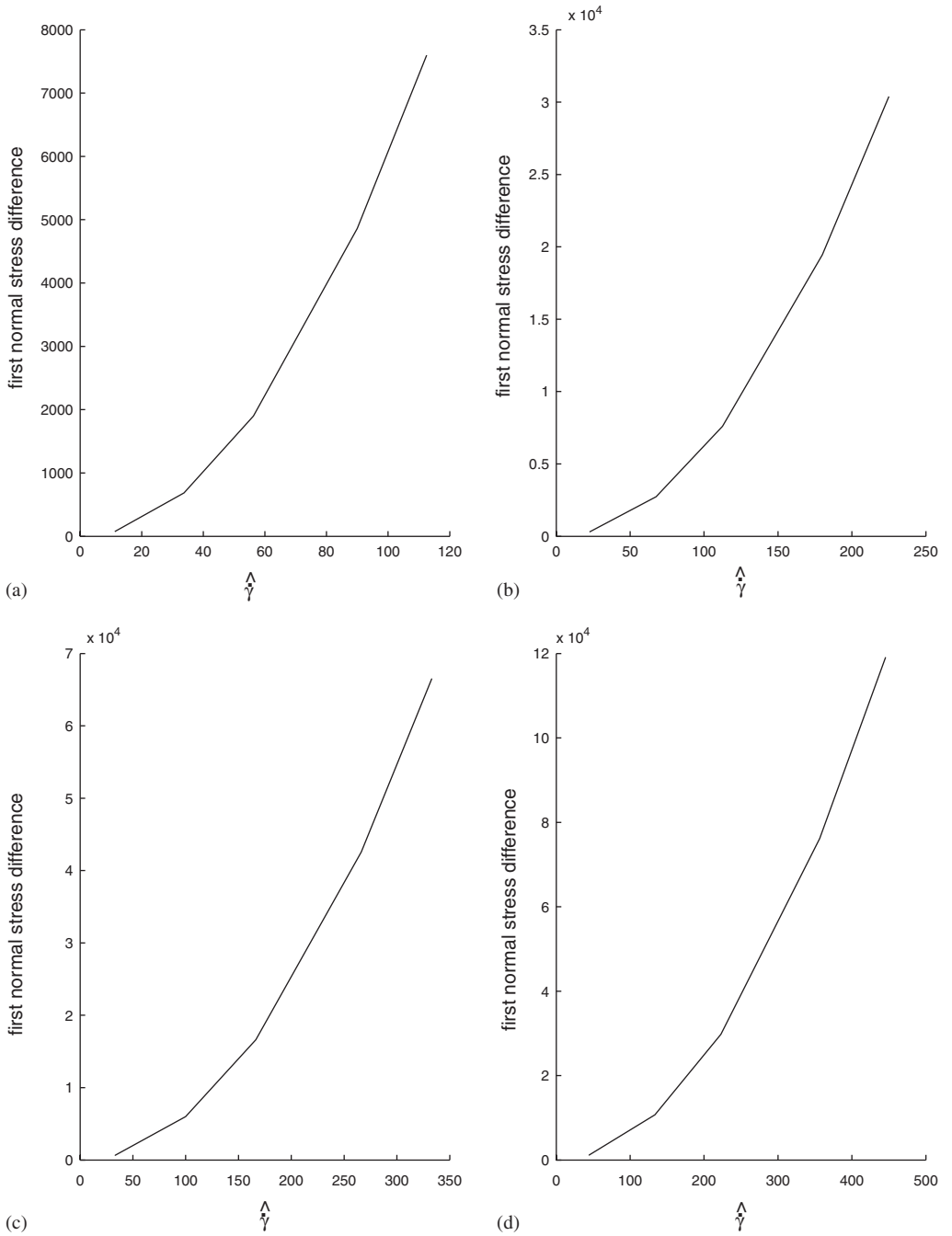

Figure 5. Fully developed flow: solutions of class c^1, $p=5$, first normal stress difference $(\hat{\tau}^e_{xx}-\hat{\tau}^e_{yy})$ versus $\hat{\dot{\gamma}}$, $\lambda_2=0.05$: (a) first normal stress difference versus $\hat{\dot{\gamma}}$ at $y=0.25$; (b) first normal stress difference versus $\hat{\dot{\gamma}}$ at $y=0.5$; (c) first normal stress difference versus $\hat{\dot{\gamma}}$ at $y=0.75$; and (d) first normal stress difference versus $\hat{\dot{\gamma}}$ at $y=1.0$.

Copyright © 2006 John Wiley & Sons, Ltd.

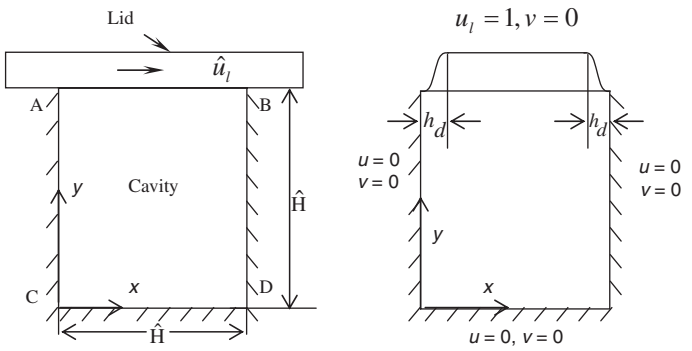

(a) $\hat{H} = 0.1m, L_0 = 0.1m, H = 1$ (b) $\hat{u}_l = u_0\ ;\ u_l = 1$

Edge	Element Lengths					
$\overrightarrow{AB}$	0.1	0.1	0.3	0.3	0.1	0.1
$\overrightarrow{CA}$	0.2	0.2	0.2	0.2	0.1	0.1

(c)

Edge	Element Lengths									
$\overrightarrow{AB}$	0.1	0.1	0.1	0.1	0.1	0.1	0.1	0.1	0.1	0.1
$\overrightarrow{CA}$	0.1	0.1	0.1	0.1	0.1	0.1	0.1	0.1	0.1	0.1

(d)

Edge	Element Lengths						
$\overrightarrow{AB}$	0.05	0.05	0.25	0.3	0.25	0.05	0.05
$\overrightarrow{CA}$	0.25	0.25	0.25	0.075	0.075	0.05	0.05

(e)

Edge	Element Lengths									
$\rightarrow$ AB	0.05	0.05	0.05	0.05	0.05	0.05	0.05	0.05	0.05	0.05
	0.05	0.05	0.05	0.05	0.05	0.05	0.05	0.05	0.05	0.05
$\rightarrow$ CA	0.05	0.05	0.05	0.05	0.05	0.05	0.05	0.05	0.05	0.05
	0.05	0.05	0.05	0.05	0.05	0.05	0.05	0.05	0.05	0.05

(f)

Figure 6. Schematic and discretizations for lid driven cavity: (a) schematic of lid driven cavity; (b) idealization of lid driven cavity in (a): computational domain and boundary conditions; (c) a 36 element discretization: mesh M1; $h_d = 0.1$; (d) a 100 element discretization: mesh M2; $h_d = 0.1$; (e) a 49 element discretization: mesh M3; $h_d = 0.05$; and (f) a 400 element discretization: mesh M4; $h_d = 0.05$.

Copyright © 2006 John Wiley & Sons, Ltd.

8.2.1. p-convergence of the solution of class C^k, k = 1,2,3. Mesh M1 (36 Ele.), De = 0.2, $h_d = 0.1$, $\lambda_2 = 0.05$. We consider a quasi-uniform mesh consisting of 36 elements with $h_d = 0.1$ and $De = 0.2$. First, we consider solutions of class C^1, i.e. local approximation in $H^{2,p}(\bar{\Omega}^e)$ space. p-levels are increased uniformly from $p = 5$ to 9 for each element of the discretization until converged solutions are obtained. A comparison of the results at $x = 0.5$, $y = 0.5$ and $y = 0.95$ shows that results for $p = 7$ and 9 are in good agreement (not shown for brevity) indicating that further increase in the p levels will not result in any appreciable change. Hence, results at $p = 9$ could be treated as a limit point for the solution of class C^1. Similar studies were conducted for solutions of class C^2 and C^3 to obtain limit points in $H^{3,p}(\bar{\Omega}^e)$ and $H^{4,p}(\bar{\Omega}^e)$ spaces. Limit points for the solution of classes C^2 and C^3 are in very close agreement everywhere (results not shown) in the cavity including the very close neighbourhood of points A and B. Thus, the limit point for the solution of class C^3 can be treated as a solution that is independent of p and k.

8.2.2. h, p, k independence of the solutions for De = 0.2, $h_d = 0.1$ and $\lambda_2 = 0.05$. In Section 8.2.1, limit points in spaces $H^{k,p}(\bar{\Omega}^e)$, $k = 2$, 3 and 4 were obtained and the fact that the limit points for $k = 3$ and 4 are in close agreement shows that limit point in space $H^{4,p}(\bar{\Omega}^e)$ is infact a solution that is independent of p and k. The studies in Section 8.2.1 were conducted for a 36 element quasi-uniform mesh with $h_d = 0.1$. Similar studies were conducted for the 100 element discretization (Mesh M2) also with $h_d = 0.1$ to obtain a solution for this mesh that is independent of p and k (i.e. limit point). Comparison of the p and k independent solutions for the two meshes with $h_d = 0.1$ is shown in Figures 7 and 8. Exceptionally good agreement between these shows mesh independence of the solution reported in Figures 7 and 8, and since these solutions are already independent of p and k, these solutions in Figures 7 and 8 are independent of h, p and k. We remark that in these solutions, the physics at the corners A and B is idealized by the velocity distribution shown in Figure 6(b) with $h_d = 0.1$ and hence these h, p, k independent solutions are for this specific value of $h_d = 0.1$.

8.2.3. h, p, k independent solutions for De = 0.2, $h_d = 0.05$ and $\lambda_2 = 0.05$. In this study we utilize 49 and 400 element meshes with $h_d = 0.05$ to obtain h, p, k independent solutions by first obtaining p, k independent solutions for the two meshes and then by comparing them to establish mesh independence of the solutions. Figures 9 and 10 show a comparison of the h, p, k independent limit points for the two meshes. A good agreement between the two indicates mesh independence of these solutions and hence h, p, k independence of the solutions.

8.2.4. Comparisons of the limit points for $h_d = 0.05$ and 0.1, De = 0.2, $\lambda_2 = 0.05$. Figures 11 and 12 show comparison of the h, p, k independent solutions for $h_d = 0.05$ and 0.1. From these results we observe that except in the immediate vicinity of corner A and B, in the rest of the cavity, the two solutions compare very well. Validity of the results in the vicinity of A and B will be discussed in the subsequent section.

8.2.5. Comparisons of the limit points for De = 0.4, $\lambda_2 = 0.05$. Studies similar to those reported for $De = 0.2$ were also conducted for $De = 0.4$ using meshes M1–M4. For $De = 0.4$ to obtain limit points for $h_d = 0.1$ and 0.05. A comparison of these limit points is shown in Figures 13 and 14. We observe behaviour similar to $De = 0.2$, i.e. except in the

Copyright © 2006 John Wiley & Sons, Ltd.

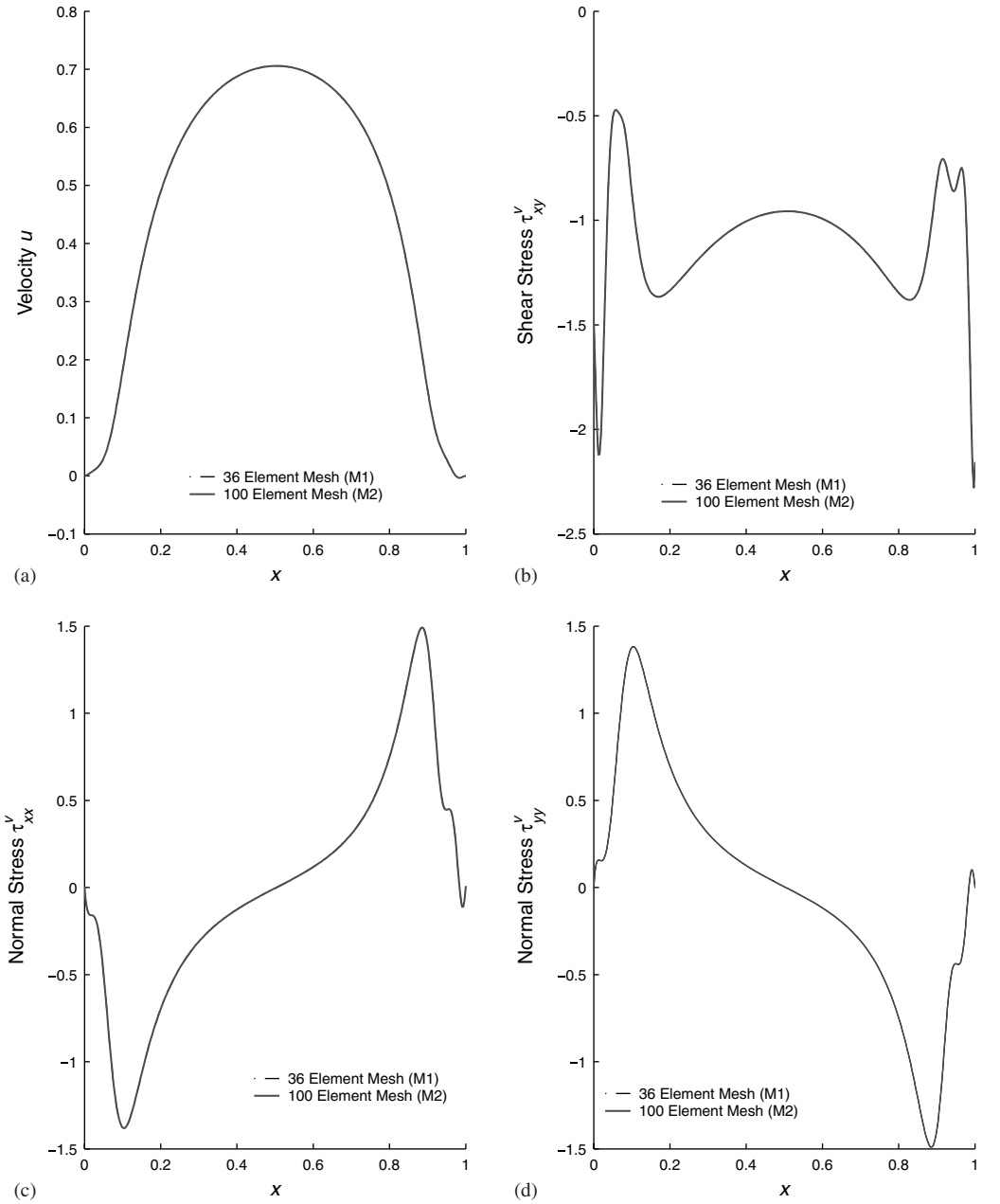

Figure 7. Comparision of p, k independent limit points for Mesh M1 and Mesh M2 at $y = 0.95$: C^3, $p = 9$, $h_d = 0.1$, $u_0 = 0.2$, $De = 0.2$, $\lambda_2 = 0.05$: (a) velocity u versus x; (b) shear stress τ^v_{xy} versus x; (c) normal stress τ^v_{xx} versus x; (d) normal stress τ^v_{yy} versus x.

Copyright © 2006 John Wiley & Sons, Ltd.

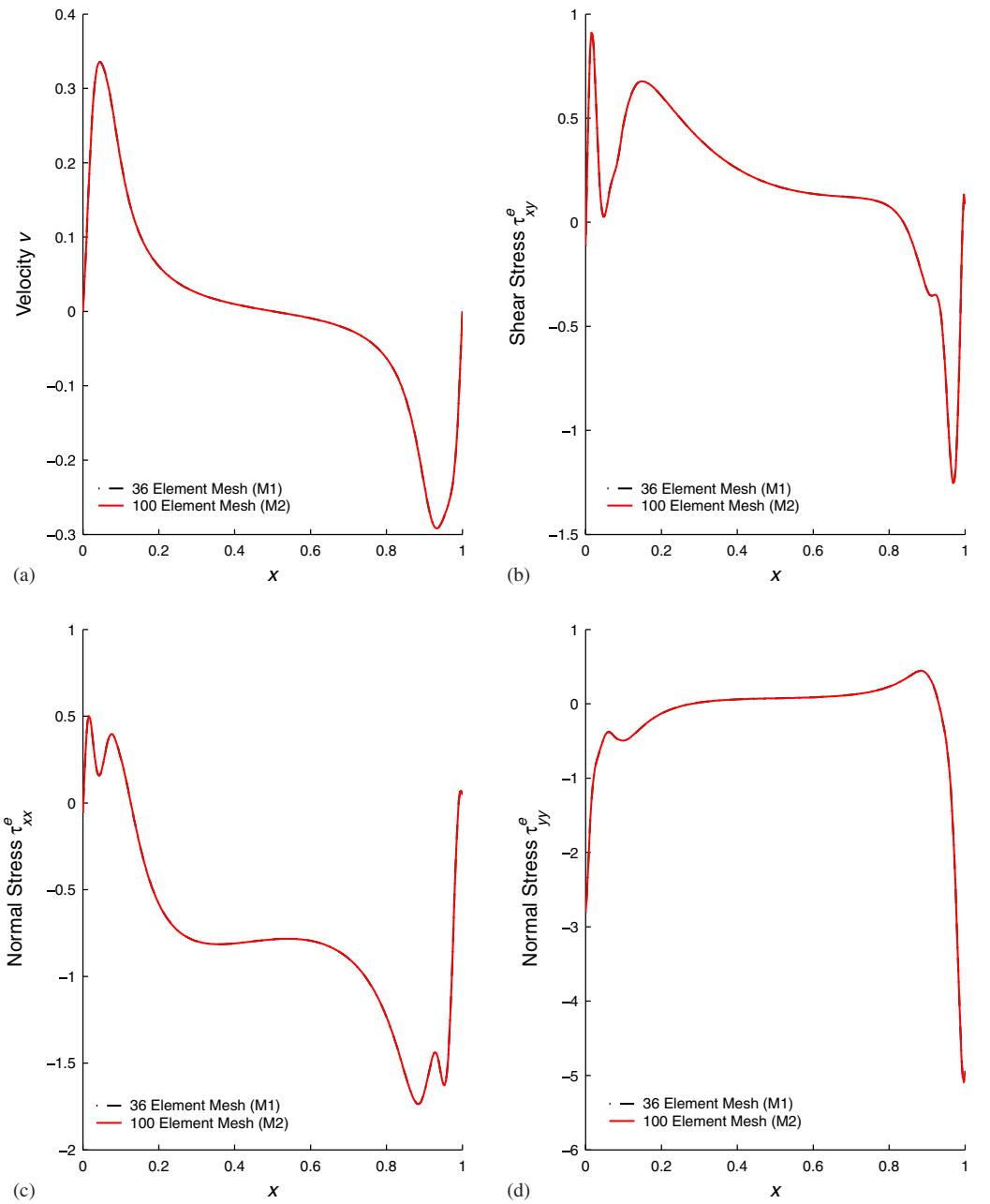

Figure 8. Comparision of p, k independent limit points for Mesh M1 and Mesh M2 at $y = 0.95$: C^3, $p = 9$, $h_d = 0.1$, $u_0 = 0.2$, $De = 0.2$, $\lambda_2 = 0.05$: (a) velocity v versus x; (b) shear stress τ^e_{xy} versus x; (c) normal stress τ^e_{xx} versus x; and (d) normal stress τ^e_{yy} versus x.

Copyright © 2006 John Wiley & Sons, Ltd.

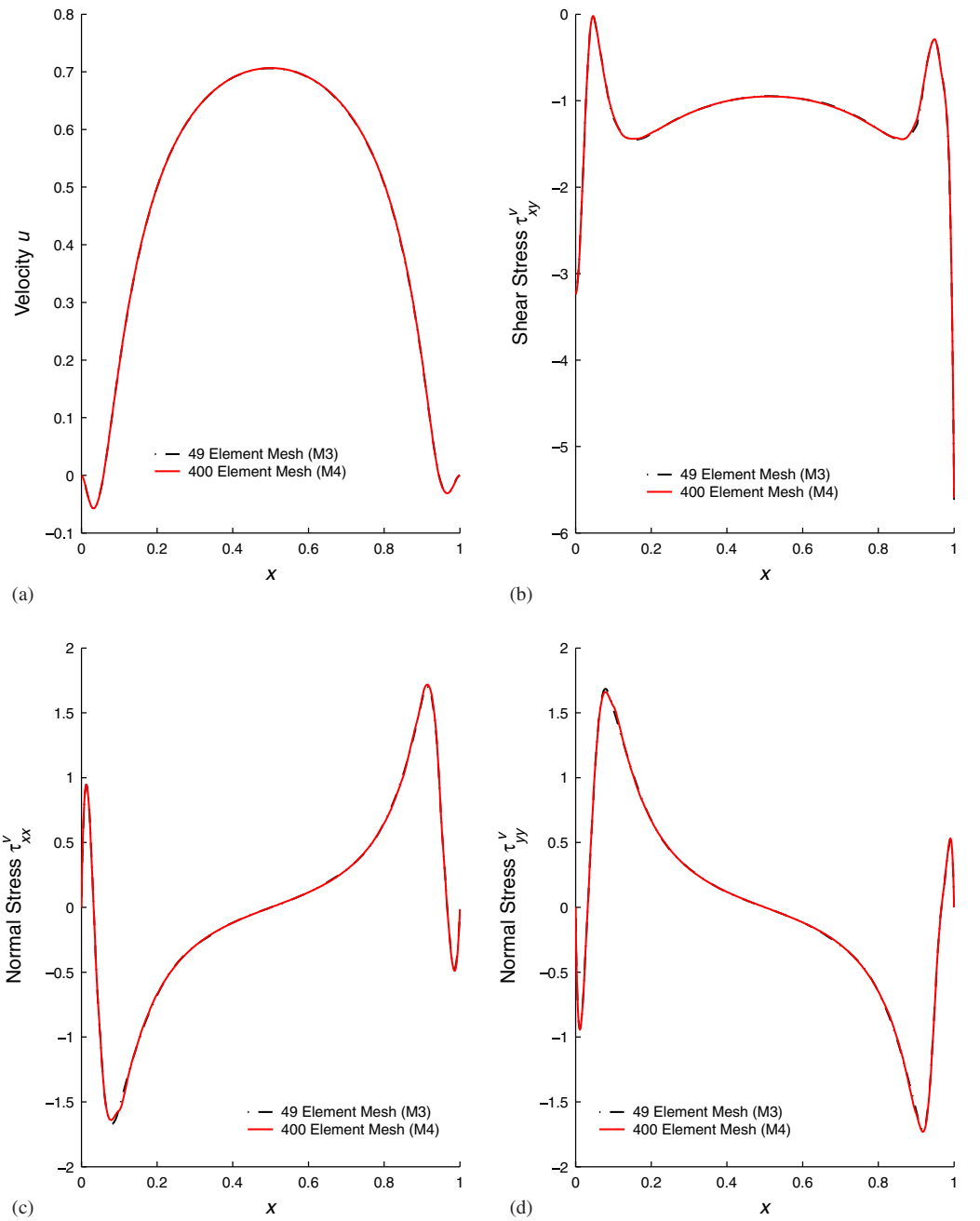

Figure 9. Comparision of p, k independent limit points for Mesh M3 and Mesh M4 at $y = 0.95$: C^3, $p = 9$, $h_d = 0.05$, $u_0 = 0.2$, $De = 0.2$, $\lambda_2 = 0.05$: (a) velocity u versus x; (b) shear stress τ^v_{xy} versus x; (c) normal stress τ^v_{xx} versus x; and (d) normal stress τ^v_{yy} versus x.

Copyright © 2006 John Wiley & Sons, Ltd.

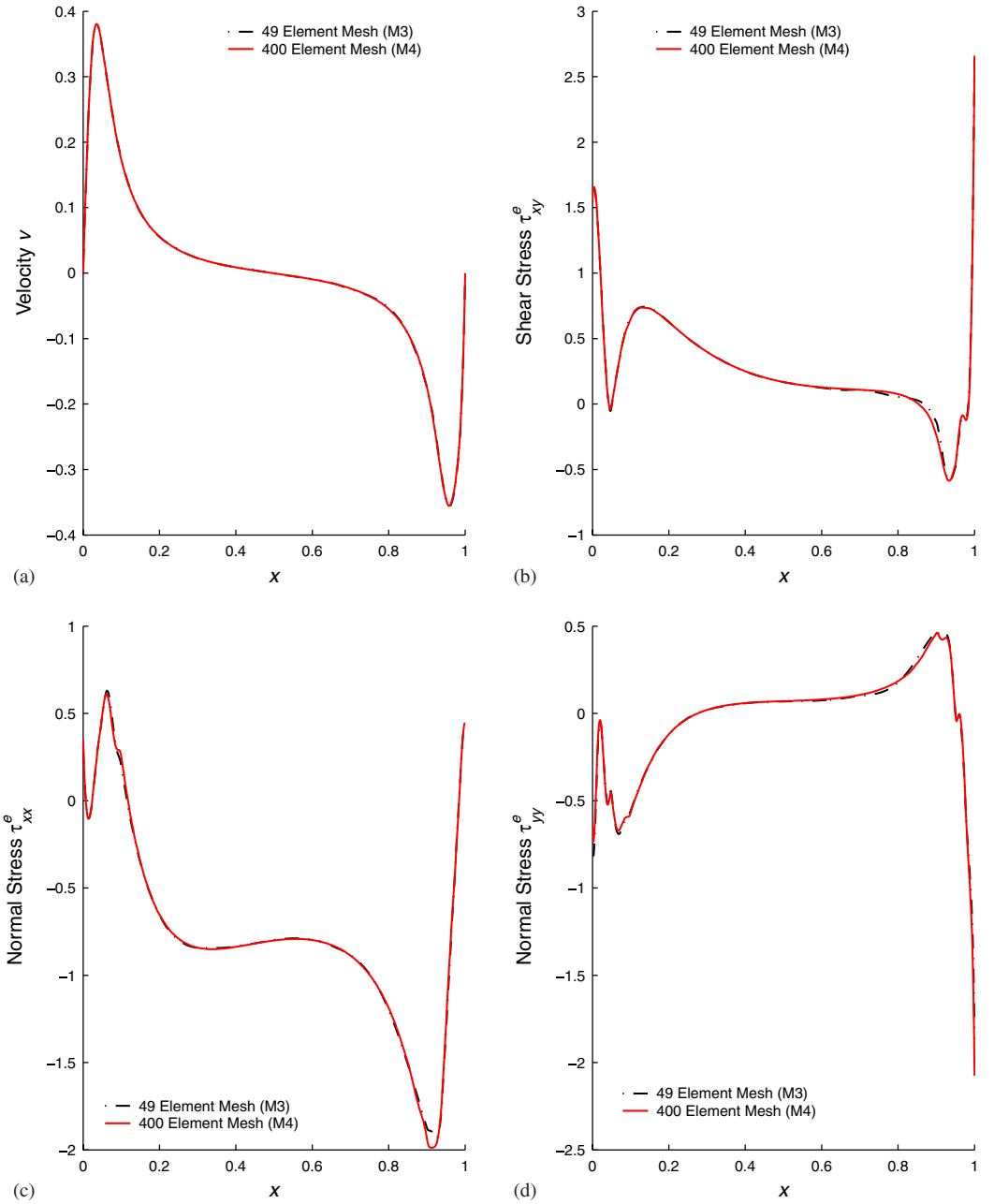

Figure 10. Comparision of p, k independent limit points for Mesh M3 and Mesh M4 at $y = 0.95$: C^3, $p = 9$, $h_d = 0.05$, $u_0 = 0.2$, $De = 0.2$, $\lambda_2 = 0.05$: (a) velocity v versus x; (b) shear stress τ^e_{xy} versus x; (c) normal stress τ^e_{xx} versus x; and (d) normal stress τ^e_{yy} versus x.

Copyright © 2006 John Wiley & Sons, Ltd.

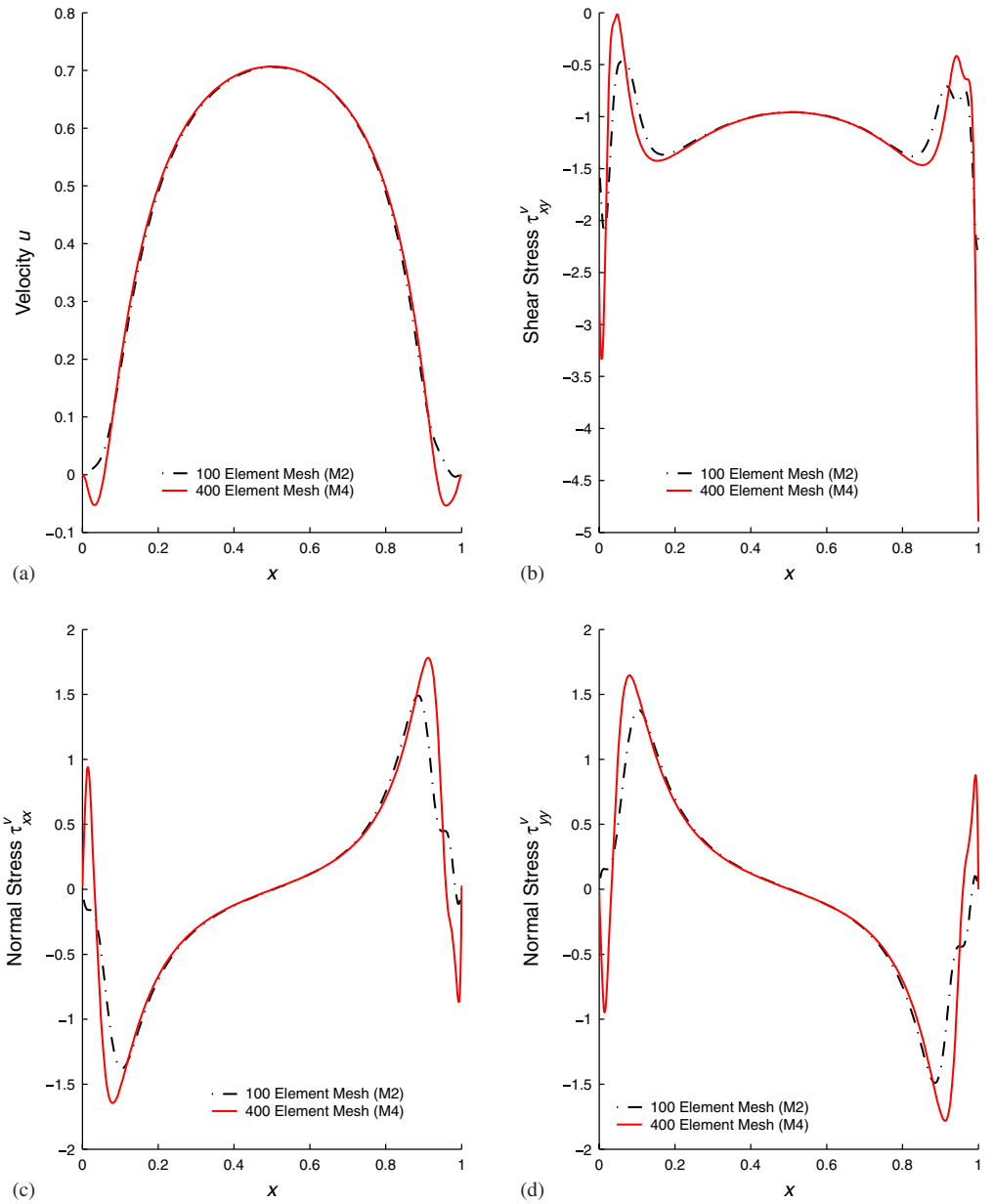

Figure 11. Comparision of h, p, k independent solutions of class C^3, $p=9$, for $h_d=0.1$ and $h_d=0.05$ at $y=0.95$: $u_0=0.2$, $De=0.2$, $\lambda_2=0.05$: (a) velocity u versus x; (b) shear stress τ^v_{xy} versus x; (c) normal stress τ^v_{xx} versus x; and (d) normal stress τ^v_{yy} versus x.

Copyright © 2006 John Wiley & Sons, Ltd.

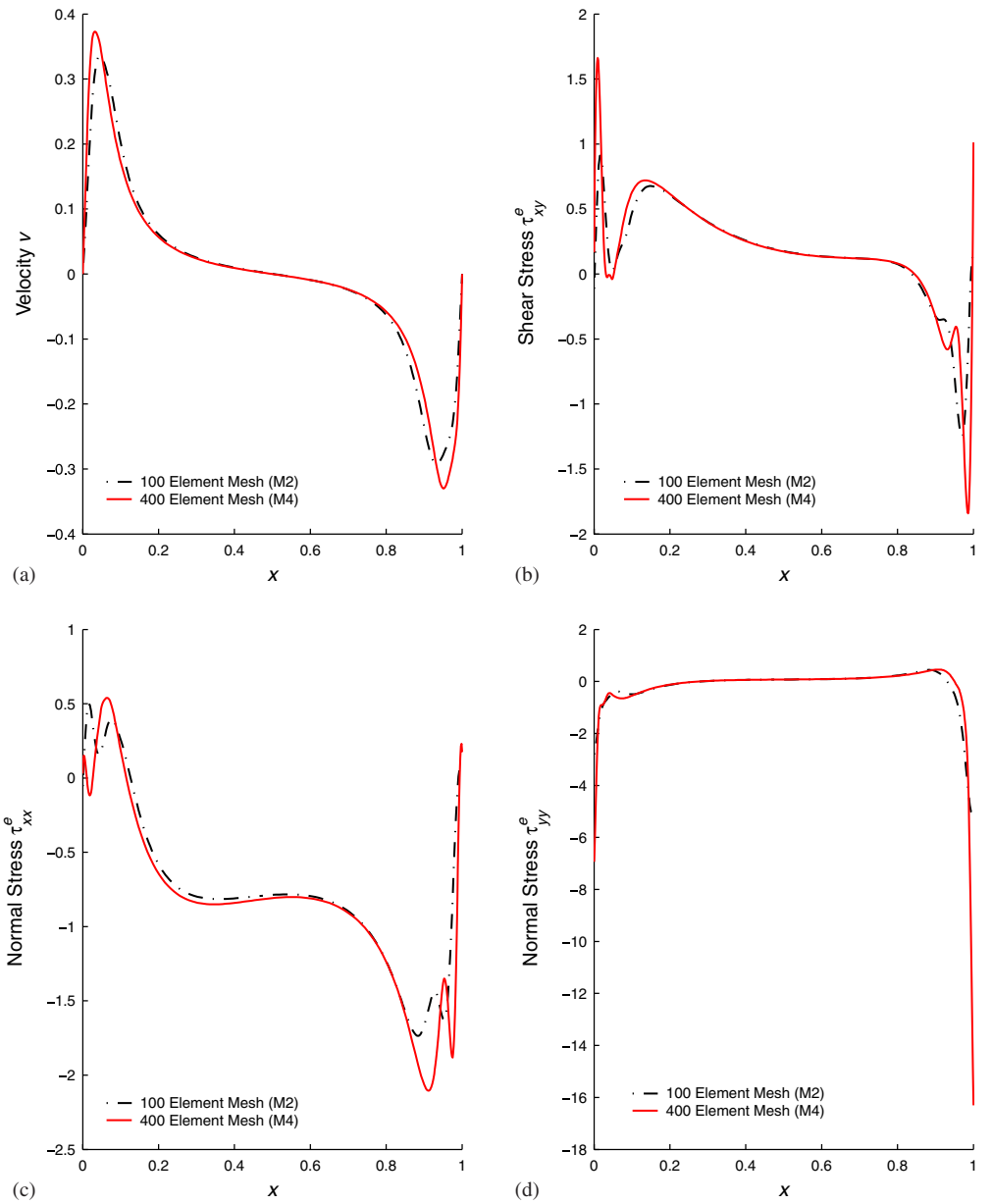

Figure 12. Comparision of h, p, k independent solutions of class C^3, $p=9$, for $h_d=0.1$ and $h_d=0.05$ at $y=0.95$: $u_0=0.2$, $De=0.2$, $\lambda_2=0.05$: (a) velocity v versus x; (b) shear stress τ^e_{xy} versus x; (c) normal stress τ^e_{xx} versus x; and (d) normal stress τ^e_{yy} versus x.

Copyright © 2006 John Wiley & Sons, Ltd.

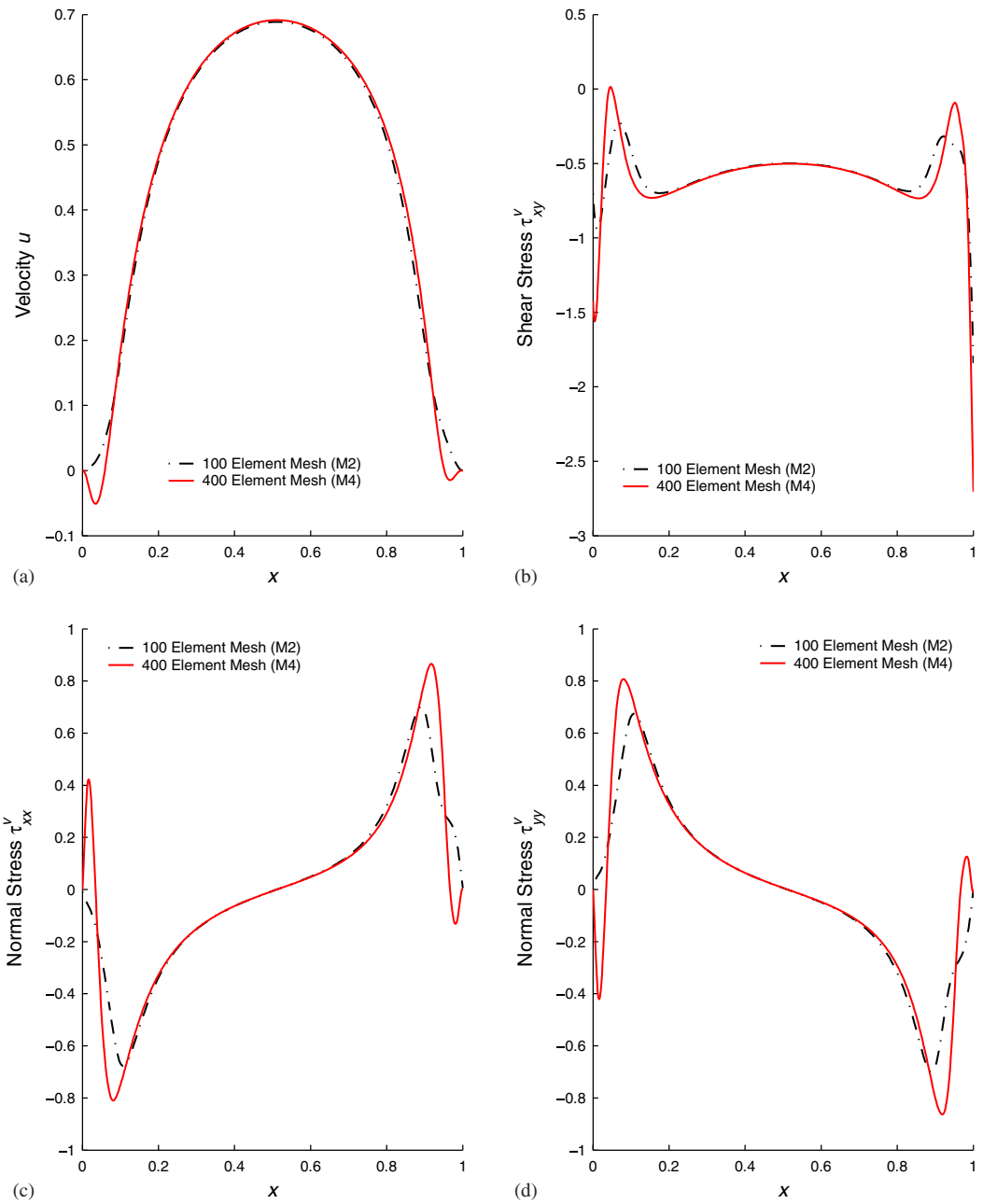

Figure 13. Comparision of h, p, k independent solutions of class C^2, $p=7$, for $h_d=0.1$ and $h_d=0.05$ at $y=0.95$: $u_0=0.4$, $De=0.4$, $\lambda_2=0.05$: (a) velocity u versus x; (b) shear stress τ^v_{xy} versus x; (c) normal stress τ^v_{xx} versus x; and (d) normal stress τ^v_{yy} versus x.

Copyright © 2006 John Wiley & Sons, Ltd.

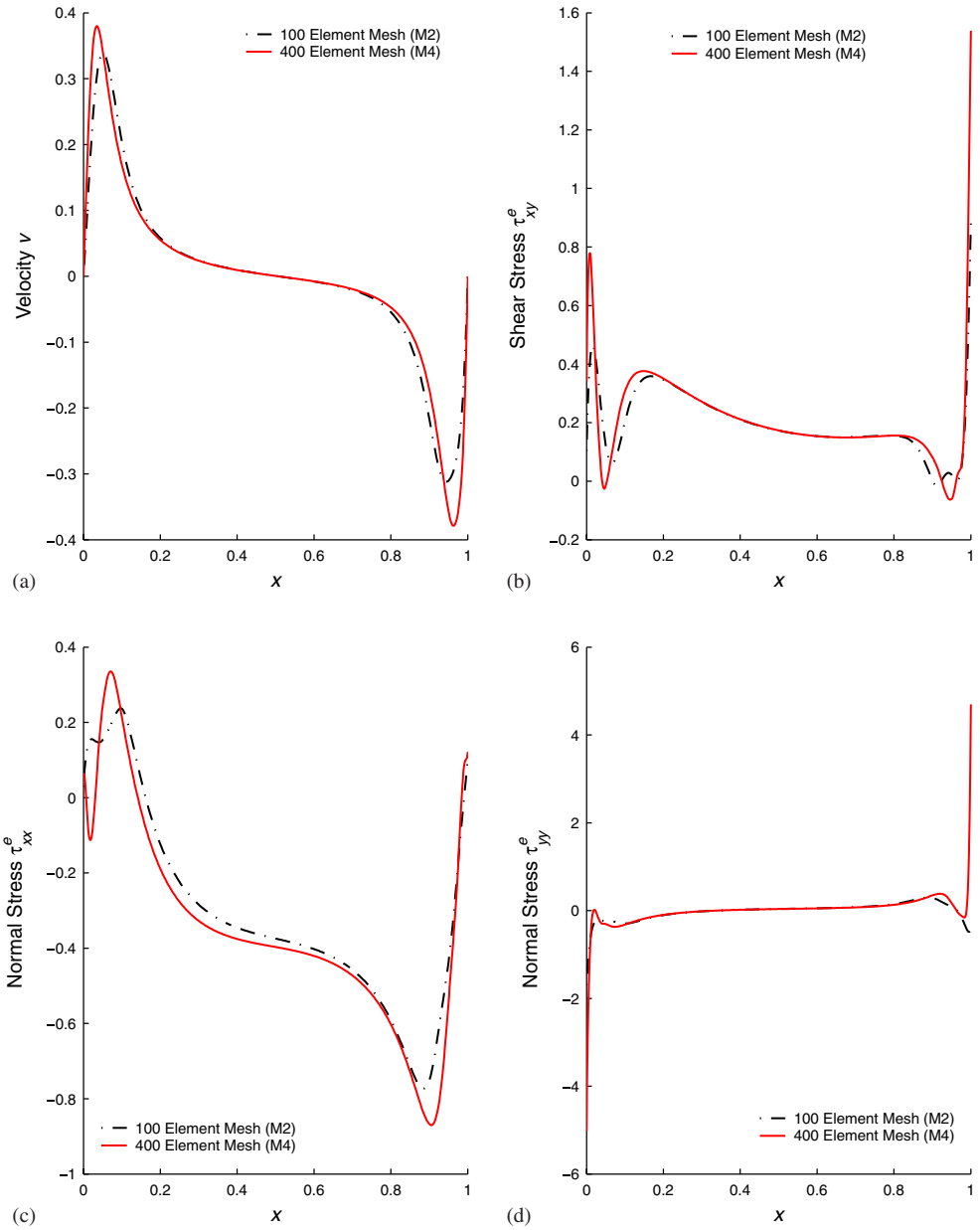

Figure 14. Comparision of h, p, k independent solutions of class C^2, $p=7$, for $h_d=0.1$ and $h_d=0.05$ at $y=0.95$: $u_0=0.4$, $De=0.4$, $\lambda_2=0.05$: (a) velocity v versus x; (b) shear stress τ^e_{xy} versus x; (c) normal stress τ^e_{xx} versus x; and (d) normal stress τ^e_{yy} versus x.

Copyright © 2006 John Wiley & Sons, Ltd.

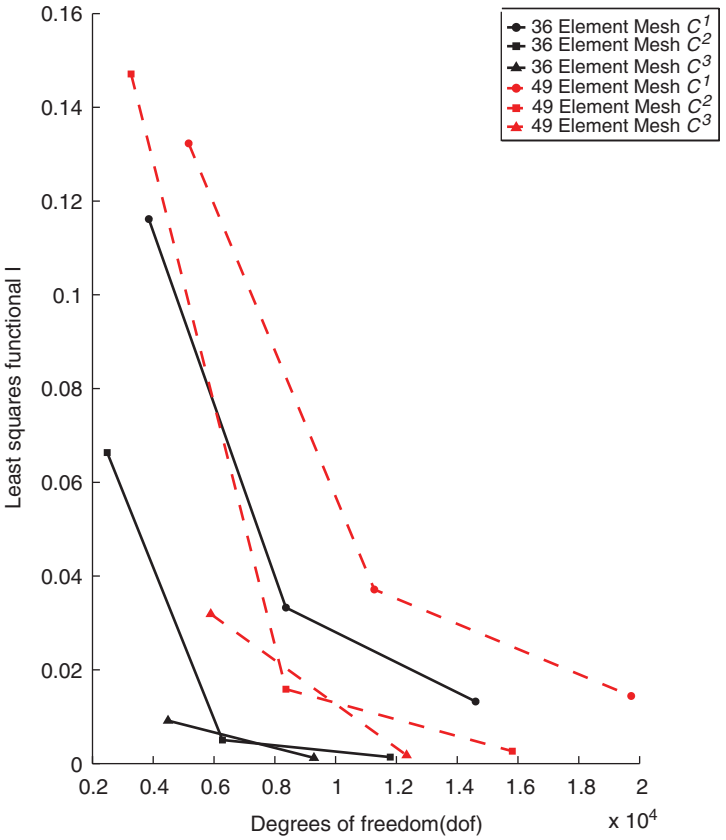

Figure 15. p-convergence of least square functional in higher order spaces.

immediate neighbourhood of the points A and B, the agreement between the two limit points for $h_d = 0.05$ and 0.1 is exceptionally good.

8.2.6. p-convergence of the least squares functional I in $H^{k,p}(\bar{\Omega}^e)$ spaces. Figure 15 shows graphs of I versus dof for meshes M1 (36 elements) and M3 (49 elements) for solutions of class C^k; $k = 1$, 2 and 3. We observe increased convergence rate with the increasing order of the space and lower values of I in the higher order spaces (for a given dof). Tables I—IV document various details of the studies presented for the meshes.

8.2.7. Converged solutions (h, p, k independent) for different values of λ_2. Solutions of class C^3 for 400 element mesh at $p = 9$ (representing h, p, k independent solutions) are shown in Figures 16–19 for $\lambda_2 = 0.0$, 0.03, 0.06 and 0.1. We note that $\lambda_2 = 0$ corresponds to Maxwell fluid and $\lambda_2 = \lambda_1$ corresponds to Newtonian fluid. First, we note that no particular difficulty is encountered for different values of λ_2. Secondly, the ability of the Oldroyd-B model to control the magnitude of stresses based on λ_2 is quite clear. By choosing appropriate value of λ_2, the model can be tuned to much lower elastic stresses than those predicted by UCMM.

Copyright © 2006 John Wiley & Sons, Ltd.

Table I. 36 Element mesh (M1).

Order of space k	p-level	Degrees of freedom	I	$\|g_i\|_{\max}$	No. of iterations
2	5	3855	1.1615E − 01	7.44E − 07	10
	7	8367	3.3270E − 02	3.40E − 07	8
	9	14 607	1.3247E − 02	1.52E − 07	9
3	5	2485	6.6342E − 02	3.42E − 07	10
	7	6277	5.0209E − 03	6.67E − 07	8
	9	11 797	1.3737E − 03	6.18E − 07	7
4	7	4487	9.9169E − 03	9.67E − 07	13
	9	9287	1.2148E − 03	3.54E − 07	7

Table II. 49 Element mesh (M3).

Order of space k	p-level	Degrees of freedom	I	$\|g_i\|_{\max}$	No. of iterations
2	5	5167	1.3231E − 01	8.69E − 07	19
	7	11 271	3.7144E − 02	8.53E − 07	15
	9	19 727	1.4414E − 02	7.25E − 07	13
3	5	3271	1.4712E − 01	4.33E − 07	16
	7	8367	1.5862E − 02	9.37E − 07	9
	9	15 815	2.6362E − 03	9.86E − 07	8
4	7	5895	3.1904E − 02	8.88E − 07	20
	9	11 335	1.7716E − 03	7.31E − 07	12

Table III. 100 Element mesh (M2).

Order of space k	p-level	Degrees of freedom	I	$\|g_i\|_{\max}$	No. of iterations
2	5	10 255	1.1528E − 01	6.59E − 07	10
3	7	16 437	1.43692E − 03	8.25E − 07	7
4	9	24 071	1.9148E − 03	3.55E − 07	7

Table IV. 400 Element mesh (M4).

Order of space k	p-level	Degrees of freedom	I	$\|g_i\|_{\max}$	No. of iterations
2	3	10 255	3.17615	9.03E − 07	39
	5	39 625	4.5027E − 01	9.58E − 07	17
3	9	62 837	4.8174E − 03	6.92E − 07	11

Copyright © 2006 John Wiley & Sons, Ltd.

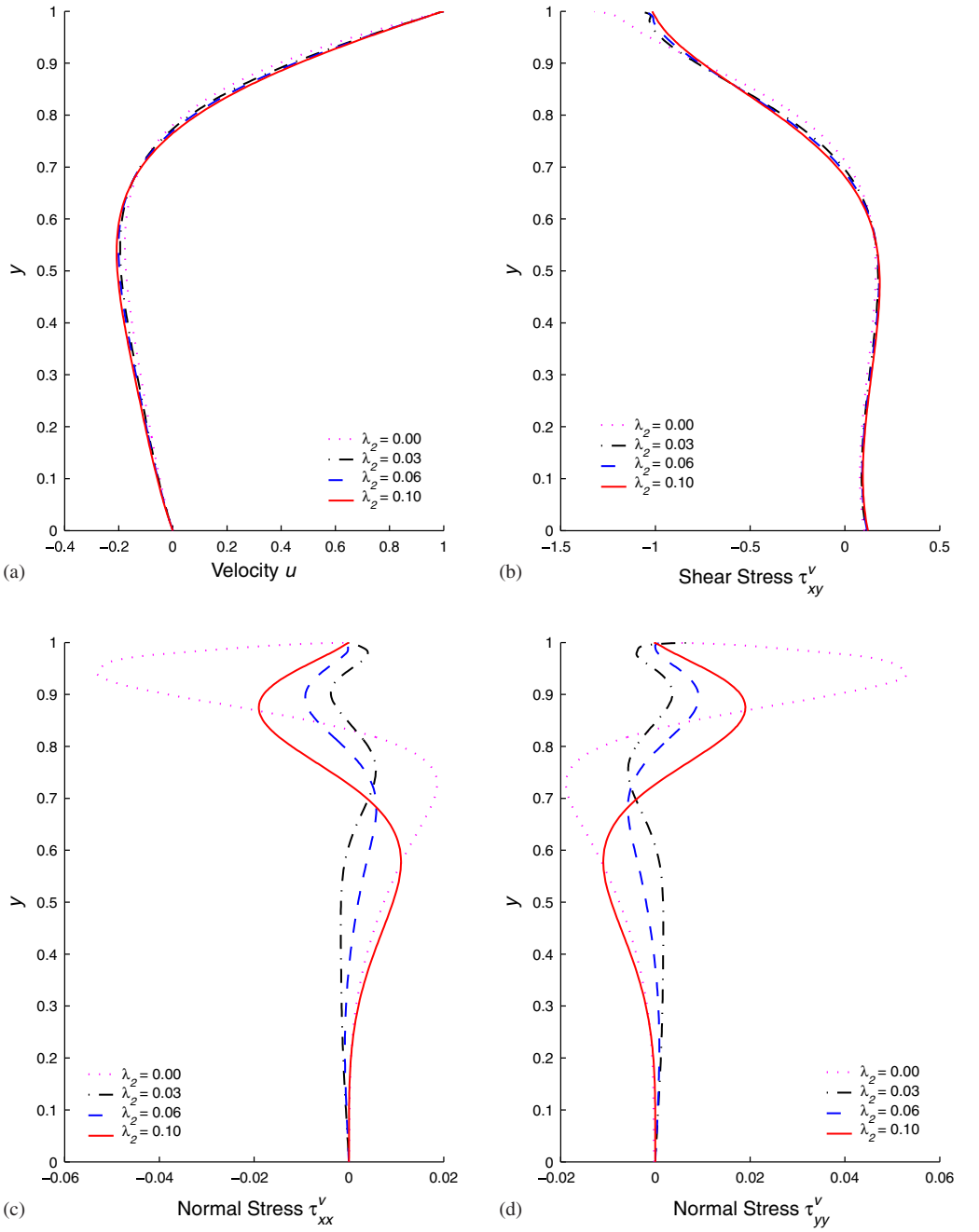

Figure 16. h, p, k independent solutions of class C^2, $p=7$, at $x=0.5$: for Mesh M4 (400 Ele.) $h_d=0.05$, $u_0=0.2$, $De=0.2$: (a) velocity u versus y; (b) shear stress τ^v_{xy} versus y; (c) normal stress τ^v_{xx} versus y; and (d) normal stress τ^v_{yy} versus y.

Copyright © 2006 John Wiley & Sons, Ltd.

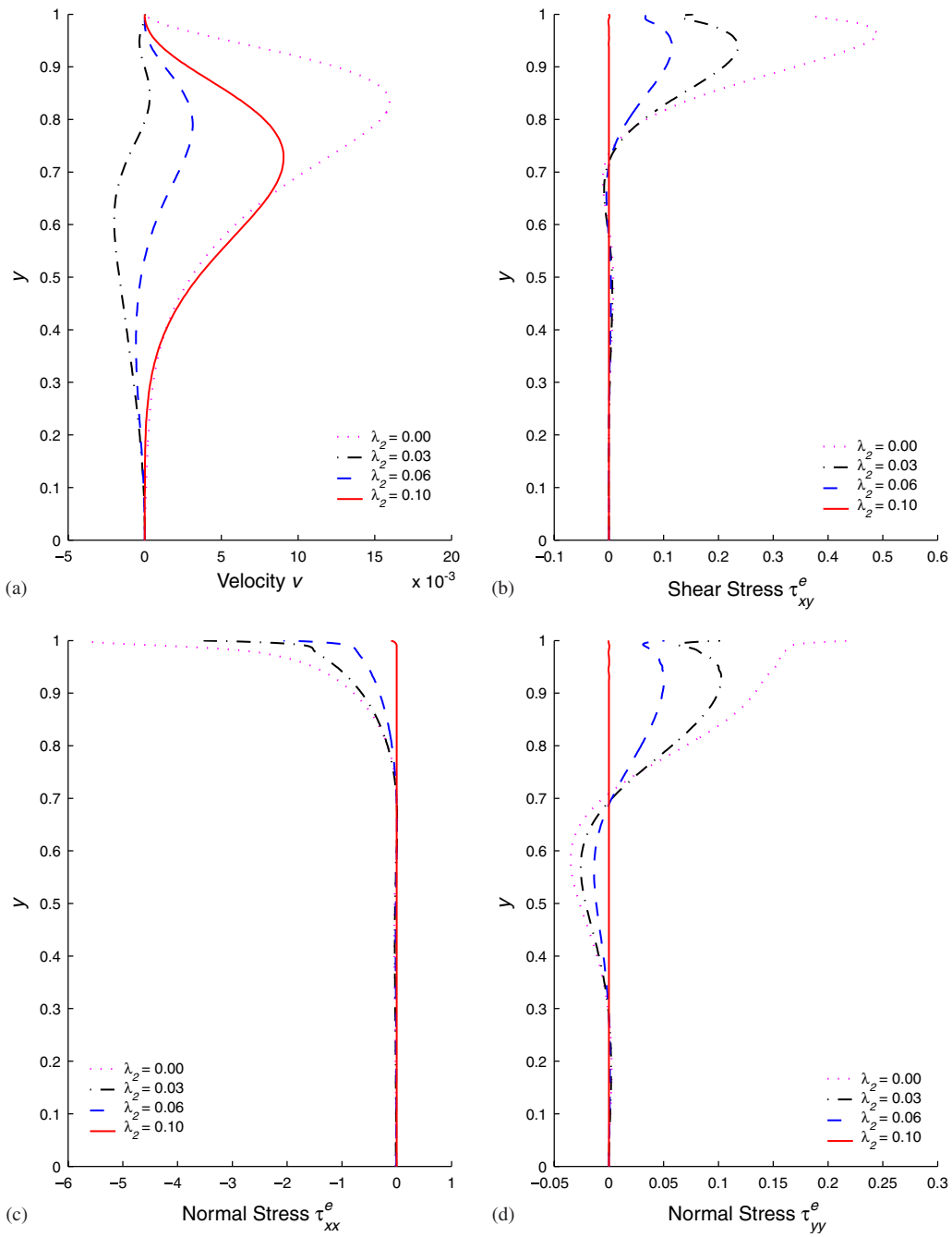

Figure 17. h, p, k independent solutions of class C^2, $p=7$, at $x=0.5$: for Mesh M4 (400 Ele.) $h_d=0.05$, $u_0=0.2$, $De=0.2$: (a) velocity v versus y; (b) shear stress τ^e_{xy} versus y; (c) normal stress τ^e_{xx} versus y; and (d) normal stress τ^e_{yy} versus y.

Copyright © 2006 John Wiley & Sons, Ltd.

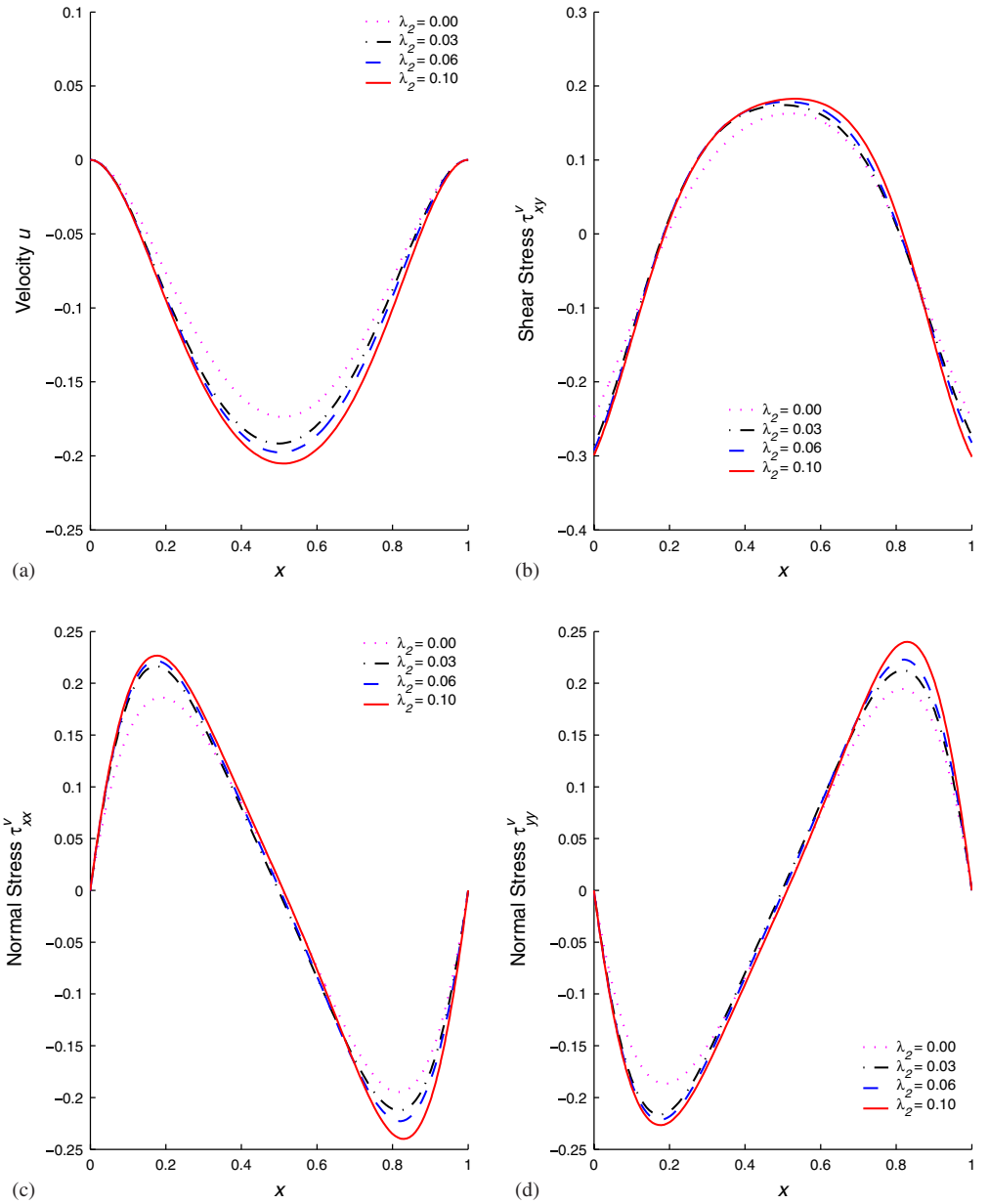

Figure 18. h, p, k independent solutions of class C^2, $p=7$, at $y=0.5$: for Mesh M4 (400 Ele.) $h_d=0.05$, $u_0=0.2$, $De=0.2$: (a) velocity u versus x; (b) shear stress τ^v_{xy} versus x; (c) normal stress τ^v_{xx} versus x; and (d) normal stress τ^v_{yy} versus x.

Copyright © 2006 John Wiley & Sons, Ltd.

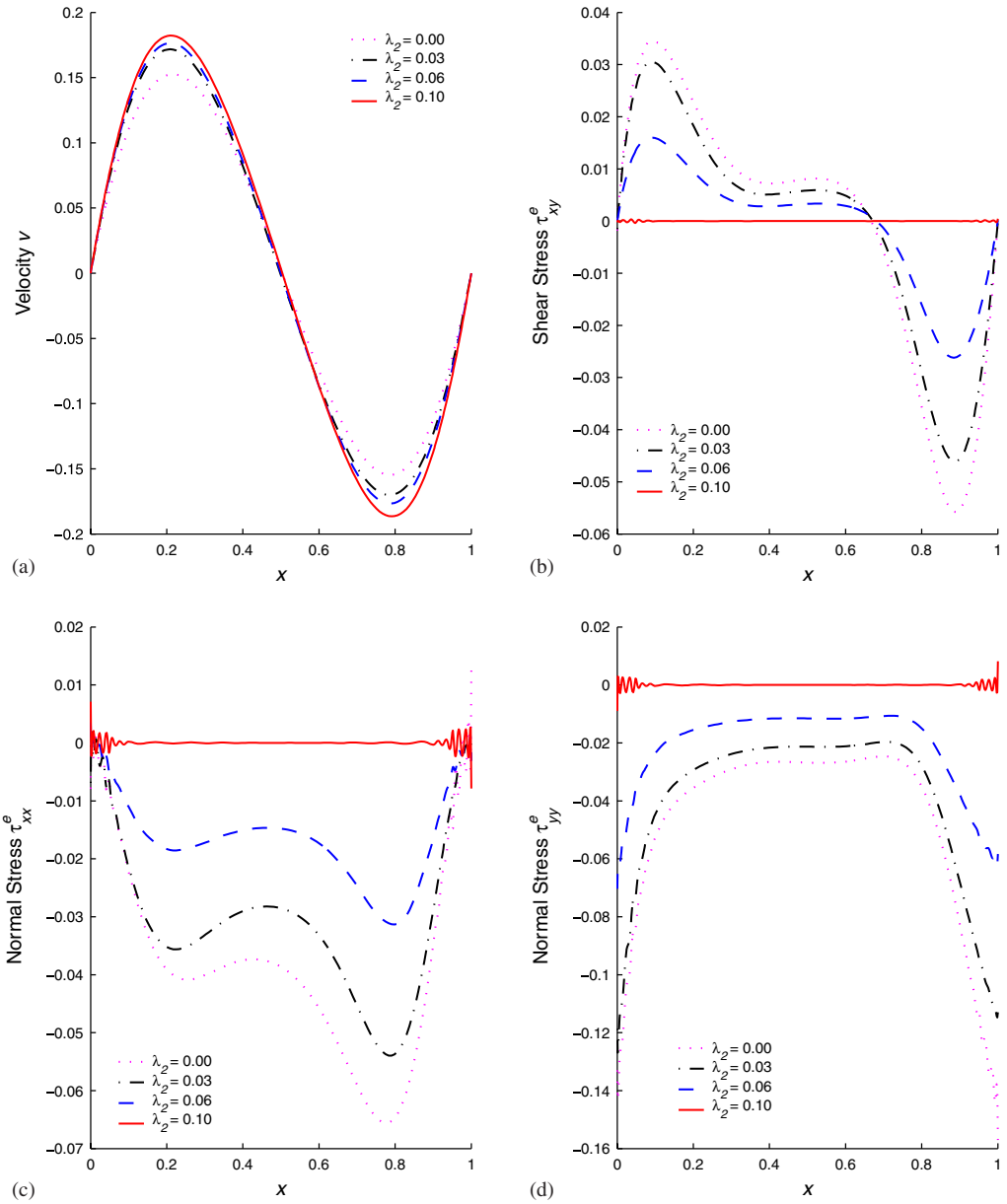

Figure 19. h, p, k independent solutions of class C^2, $p=7$, at $y=0.5$: for Mesh M4 (400 Ele.) $h_d=0.05$, $u_0=0.2$, $De=0.2$: (a) velocity v versus x; (b) shear stress τ^e_{xy} versus x; (c) normal stress τ^e_{xx} versus x; and (d) normal stress τ^e_{yy} versus x.

Copyright © 2006 John Wiley & Sons, Ltd.

The Oldroyd-B model has a much bigger range of $\hat{\dot{\gamma}}$ than UCMM. Based on experimental work reported in Reference [38], $\hat{\dot{\gamma}}$ of upto 3 would yield reasonable agreement between the Oldroyd-B model and the experiments.

8.2.8. Discussion of results. Here we present a discussion of the results reported in Sections 8.2.1–8.2.7 for lid driven cavity for $De = 0.2$ and 0.4 with $h_d = 0.05$ and 0.1.

(1) First, we note that h, p, k independence of the solutions for $h_d = 0.1$ and 0.05 are in exceptionally good including the near vicinity of points A and B.
(2) The limit points for $h_d = 0.1$ and 0.05 also agree well with each other except in the very close vicinity of points A and B.
(3) Thus, we have converged solutions that are independent of h, p and k except in the very close neighbourhood of points A and B with changing h_d. We believe, it is important to discuss what these solutions mean in terms of correlation with experiments as well as satisfying GDEs.
(4) Since the Oldroyd-B model is only good for dilute polymer solutions and its range of validity established based on experiments [38] show that the model only produces results with reasonable agreement with experiments for low values of $\hat{\dot{\gamma}}$ ($\hat{\dot{\gamma}} \leqslant 3$). Hence, first thing we need to do is to examine $\hat{\dot{\gamma}}$ through out the cavity for various solutions. Corresponding to the limit points for all four meshes, distributions of $\dot{\gamma}$ is shown for $x = 0.5$, $y = 0.95$, 0.75, 0.5, 0.4, 0.3, 0.2, 0.1. For $L_0 = 0.1$, $u_0 = 0.2$ and $De = 0.2$ (Figures 20 and 21) we have $\dot{\gamma} = 1.5$ (corresponding to the limiting value of $\hat{\dot{\gamma}} = 3$). We observe that except in the small portion of the cavity far away from the lid, $\dot{\gamma}$ values far exceed the permissible value of $\dot{\gamma}$ for Oldroyd-B model. Conforming that the numerical results reported here (though represent limit points) will not be in agreement with the experiments. Similar graphs for $De = 0.4$ are shown in Figures 22 and 23 with behaviours similar to $De = 0.2$ except that in this case due to higher Deborah number and hence increased elasticity, only a relatively smaller portion of the cavity (compared to $De = 0.2$) shows permissible range of $\dot{\gamma}$.
(5) From Tables I–IV, we observe that inspite of attempts to refine the meshes, increasing p-levels as well as increasing the order of the space, the least squares functional (I) values remain in the range (10^{-1}–10^{-2}) indicating that the GDEs are not satisfied accurately by these solutions in the point-wise sense. A closer examination of the residuals resulting from the various equations indicate the constitutive equations to have the highest residuals only in the vicinity of points A and B. Away from the immediate neighbourhoods of points A and B, the GDEs satisfied quite well (I^e of the order of (10^{-5}) or lower). We note that in this model problem the flow is fully two-dimensional, i.e. all four velocity gradients exist and are non-zero in the interior of the cavity. Furthermore, the velocity gradients in the neighbourhood of the points A and B are quite high (indicated by high values of $\dot{\gamma}$) where the Oldroyd-B model is not valid. High values of I^e (element residuals) in such areas indicates that the computed solutions does not satisfy the GDEs with high precision (accurately). From the considerations of the equilibrium of a fluid control volume one could show that non-zero τ^e_{yy} is essential for its equilibrium which the Oldroyd-B model cannot produce in a manner that is consistent with the correct physics of two-dimensional elasticity.

Copyright © 2006 John Wiley & Sons, Ltd.

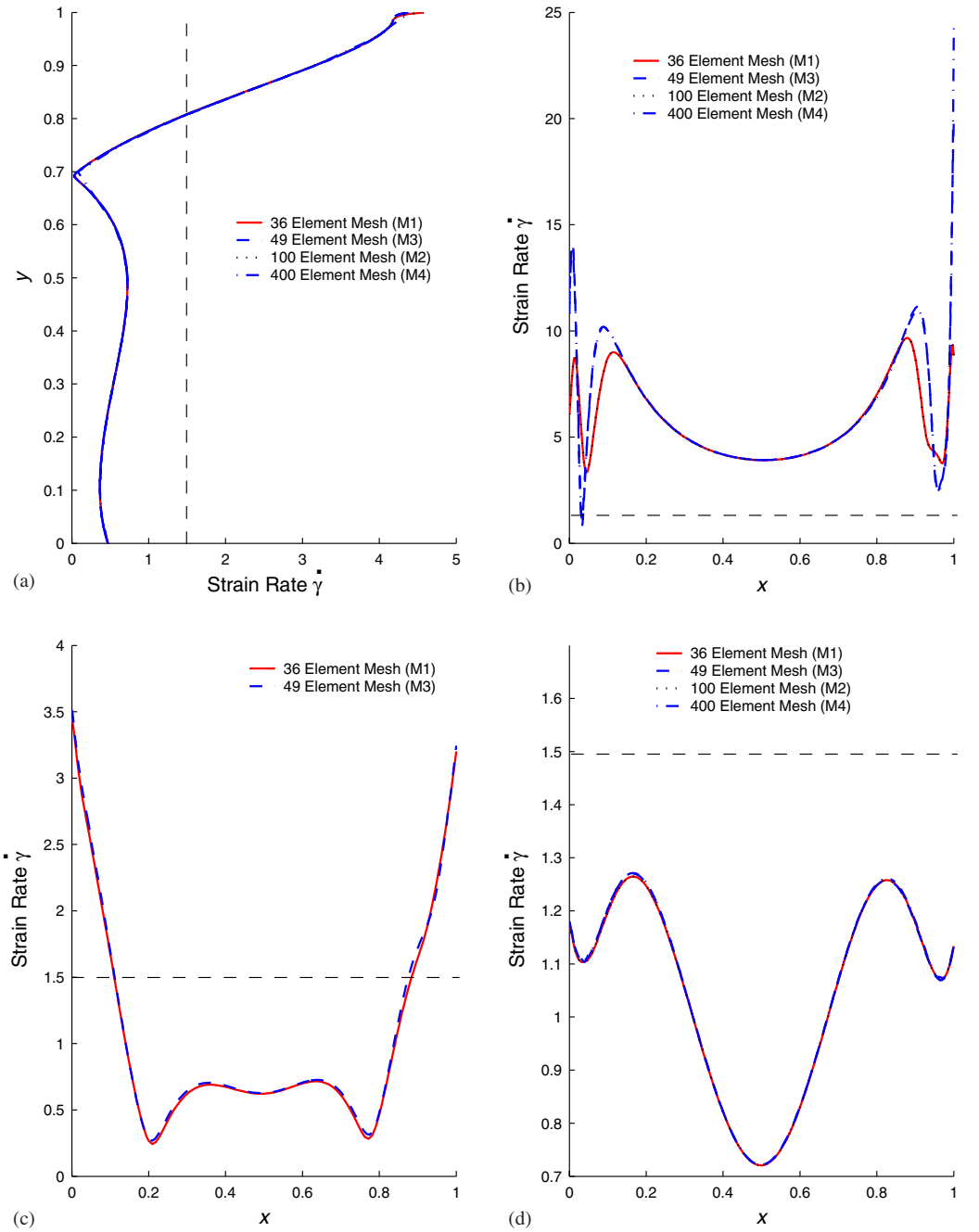

Figure 20. Strain rate at different y locations, for $h_d = 0.1$ and 0.05, C^3, $p = 9$, $De = 0.2$, $\lambda_2 = 0.05$: (Note: the dotted line represents the theoretical limit of $\dot{\gamma} = 1.5$ for this model.) (a) strain rate $\dot{\gamma}$ at $x = 0.5$; (b) strain rate $\dot{\gamma}$ at $y = 0.95$; (c) strain rate $\dot{\gamma}$ at $y = 0.75$; and (d) strain rate $\dot{\gamma}$ at $y = 0.5$.

Copyright © 2006 John Wiley & Sons, Ltd.

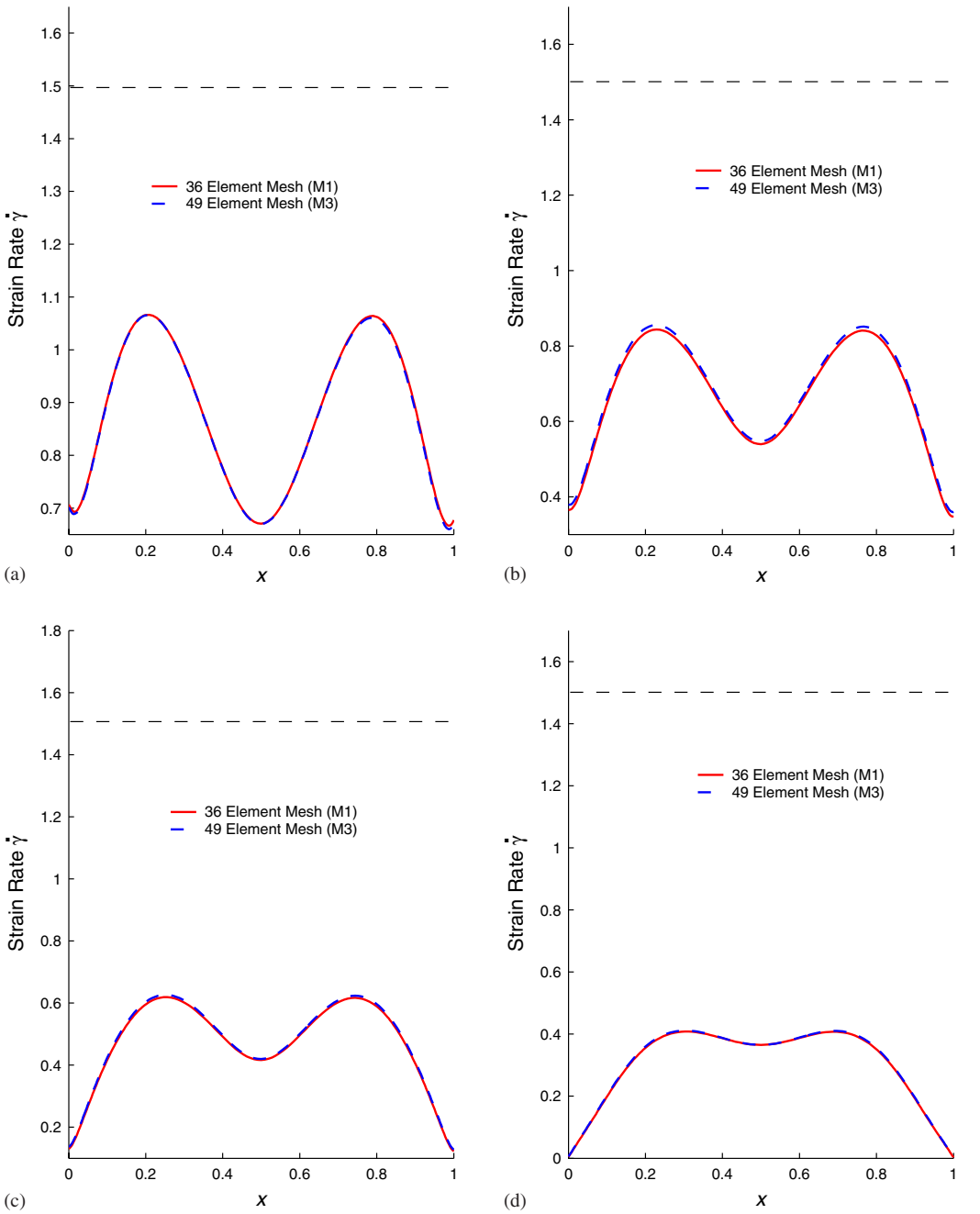

Figure 21. Strain rate at different y locations, for $h_d = 0.1$ and 0.05, C^3, $p = 9$, $De = 0.2$, $\lambda_2 = 0.05$: (Note: the dotted line represents the theoretical limit of $\dot{\gamma} = 1.5$ for this model.) (a) strain rate $\dot{\gamma}$ at $y = 0.4$: (b) strain rate $\dot{\gamma}$ at $y = 0.3$; (c) strain rate $\dot{\gamma}$ at $y = 0.2$; and (d) strain rate $\dot{\gamma}$ at $y = 0.1$.

Copyright © 2006 John Wiley & Sons, Ltd.

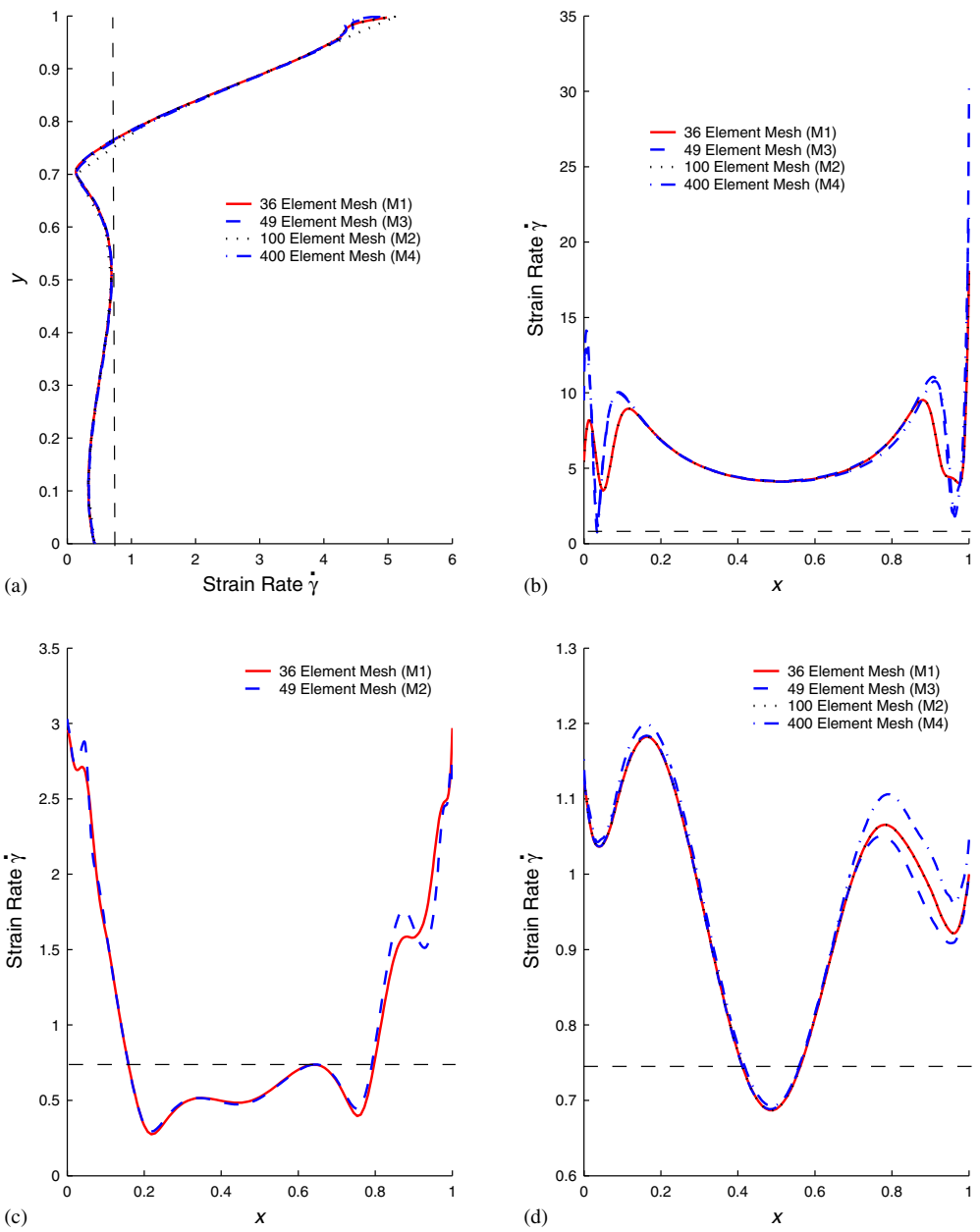

Figure 22. Strain rate at different y locations, for $h_d = 0.1$ and 0.05, C^3, $p = 9$, $De = 0.4$, $\lambda_2 = 0.05$: (Note: the dotted line represents the theoretical limit of $\dot{\gamma} = 0.75$ for this model.) (a) strain rate $\dot{\gamma}$ at $x = 0.5$; (b) strain rate $\dot{\gamma}$ at $y = 0.95$; (c) strain rate $\dot{\gamma}$ at $y = 0.75$; and (d) strain rate $\dot{\gamma}$ at $y = 0.5$.

Copyright © 2006 John Wiley & Sons, Ltd.

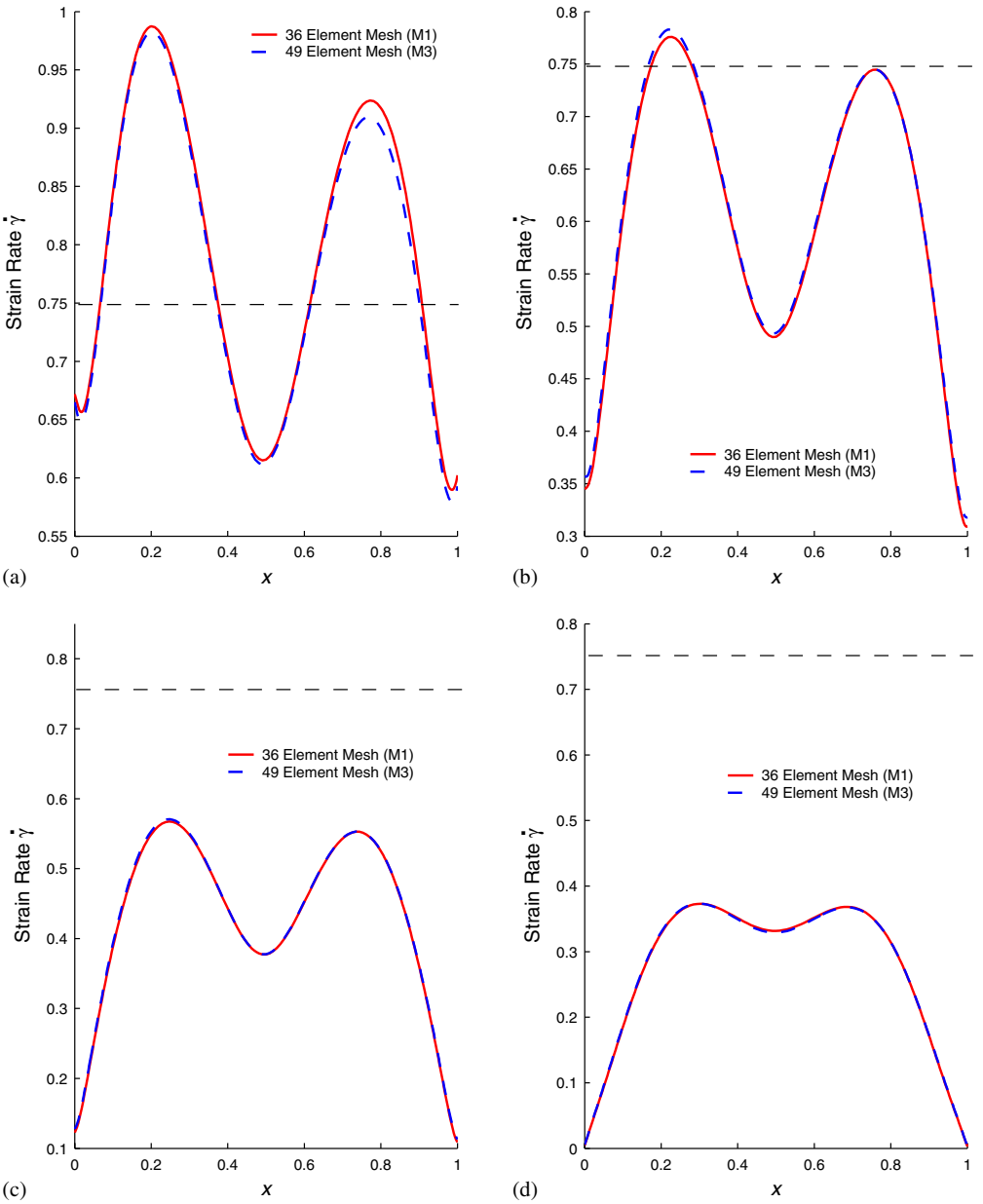

Figure 23. Strain rate at different y locations, for $h_d = 0.1$ and 0.05, C^3, $p = 9$, $De = 0.4$, $\lambda_2 = 0.05$: (Note: the dotted line represents the theoretical limit of $\dot{\gamma} = 0.75$ for this model.) (a) strain rate $\dot{\gamma}$ at $y = 0.4$; (b) strain rate $\dot{\gamma}$ at $y = 0.3$; (c) strain rate $\dot{\gamma}$ at $y = 0.2$; and (d) strain rate $\dot{\gamma}$ at $y = 0.1$.

Copyright © 2006 John Wiley & Sons, Ltd.

(6) As Deborah number is increased from 0.2 to 0.4, the spuriousness in the solution in the neighbourhood of points A and B grows and the size of its domain increases as well. For Deborah numbers greater than 0.4 the size of the domain of spurious solution will progressively increase, eventually contaminating the solution in the entire cavity and resulting in the failure of computations (failure of Newton's method with line search). It is for this reason that computations beyond $De = 0.4$ are not reported as they are meaningless due to: (a) extremely high values of $\dot{\gamma}$ than permissible for the Oldroyd-B model; (b) lack of the physics of two-dimensional elasticity which leads to erroneous solutions specially in the areas of high $\dot{\gamma}$. It is worth remarking regarding the robustness of the proposed computational framework. Even though in the numerical studies for both values of De number Oldroyd-B model is spurious due to shear rates well beyond its range of validity but, the proposed approach permits computations that try to satisfy GDE.

(7) Studies were also conducted for GDEs in u, v, p, $\boldsymbol{\tau}^e$. These studies show no benefits over GDEs in u, v, p, $\boldsymbol{\tau}$ and hence not reported here.

9. SUMMARY AND CONCLUSIONS

In this paper, the new mathematical framework presented by Surana *et al.* [25–27] based on h, p, k and variational consistency of the integral forms is utilized to develop a finite element computational process for 2-D steady polymer flows utilizing Oldroyd-B constitutive model. In the following, we present a summary of the work and draw some conclusions.

(1) First, the choice of dependent variables in the GDEs is discussed. While, there are many alternatives possible, it is shown that the mathematical characteristics of the computational process remain unaffected by these choices due to the fact that GDEs remain non-linear, thus Galerkin method with weak form remain VIC where as LSP always yield VC integral forms regardless of the nature of non-linear partial differential equations. We argue that a most prudent choice is one that yields most simplified form of the GDEs that are free of redundancies and inconsistencies. Using u, v, p, $\boldsymbol{\tau}$ (total stress) as dependent variables yields GDEs that are in the strong from and conform to these guidelines and hence are the form of the GDEs of choice.

(2) The GDEs in u, v, p and $\boldsymbol{\tau}$ are a set of non-linear partial differential equations. We remark, that other choices of dependent variables also lead to sets of non-linear partial differential equations. Following Surana *et al.* [25–27], the finite element processes based on Galerkin method and Galerkin method with weak from are VIC. The coefficient matrices in both processes are non-symmetric and hence may lead to partial or completely complex basis and thus resulting computational processes may yield spurious solutions [33, 34]. Since the VC of the VIC integral forms cannot be restored through any justifiable mathematical means, these computational processes always have possibility of spuriousness and failure regardless of the choice of dependent variables.

(3) The elastic-viscous stress decompositions yielding GDEs in u, v, p, and $\boldsymbol{\tau}^e$ are also a system of non-linear partial differential equations in which the coefficient matrices are non-symmetric for both Galerkin and Galerkin method with weak form. This choice

Copyright © 2006 John Wiley & Sons, Ltd.

of variables presents no special benefits in the proposed frame work based on h, p, k requiring variationally consistent integral forms.

(4) It is shown that finite element processes based on LSP utilizing strong form of the GDEs in u, v, p, $\boldsymbol{\tau}$ are variationally consistent. The resulting coefficient matrices are always symmetric and hence always have a real basis and therefore the resulting computational process is inherently non-spurious and unconditionally non-degenerate.

(5) Minimally conforming spaces for local approximations are discussed. With u, v, p, $\boldsymbol{\tau}$ as variables $H^{k,p}(\bar{\Omega}^e_{xy})$; $k \geqslant 3$ spaces in which $k = 3$ is the minimally conforming space are essential for continuity of the integrand in the integral forms. If we permit weak convergence of the highest order derivatives (which is ok if the solutions are sufficiently smooth), then $k = 2$ could be viewed as minimally conforming space. Need for spaces of order higher than 3 is necessitated if one requires convergence of the higher order derivatives of the computed solutions to their theoretical values. When the theoretical solutions are not known, one obtains the limit points in various order spaces (highest order space determined by the convergence of the highest order derivatives desired) for different discretizations to arrive at a solution that is the limit point of the converging sequence of limit points and hence independent of h, p and k.

(6) Numerical studies have been presented for: (i) fully developed flow between parallel plates and (ii) lid driven square cavity. Specific findings and conclusions are presented in the following.

(7) For fully developed flow between parallel plates, a five element uniform discretization suffices for De upto 314.96 and beyond. In this case numerical solutions are possible for all values of $\hat{\dot{\gamma}}$ (beyond the range of validity for the Oldroyd-B model). It is shown that due to equilibrium of elementary fluid volume in the absence of $\hat{\tau}^e_{yy}$ computations are possible for virtually any flow rate and hence for any $\hat{\dot{\gamma}}$. $\hat{\tau}^e_{yy} = 0$ for $De \neq 0$ is non-physical and is in contradiction with experimental evidence. When $\hat{\dot{\gamma}}$ is small ($\leqslant 3$) $\hat{\tau}^e_{yy}$ is also small compared to $\hat{\tau}^e_{xx}$ and hence the first normal stress difference ($\hat{\tau}^e_{xx} - \hat{\tau}^e_{yy}$) is not effected significantly even when $\hat{\tau}^e_{yy} = 0$ and thus for $\hat{\dot{\gamma}} \leqslant 3$, the results for Oldroyd-B model may be viewed acceptable. It is important to note that for this simple case numerical simulations are possible even for those $\hat{\dot{\gamma}}$ values that are well beyond the range of validity of Oldroyd-B model even though the computed solutions are erroneous when compared with experiments. The reason for the successful simulations of course is the fact that even when $\hat{\tau}^e_{yy} = 0$, fluid volume equilibrium is possible. In two-dimensional flows in which all velocity gradients are non-zero, fluid volume equilibrium may force erroneous values of $\hat{\tau}^e_{yy}$ to be developed and thereby contaminating the solution.

(8) Extensive numerical studies have been presented for the lid driven cavity. A valid mechanism of incorporating the physics of boundary conditions at the points where the stationary walls meet the lid is proposed when the local approximations are in the higher order spaces. Numerical studies are presented for $De = 0.2$ and 0.4. It is shown that h, p, k independent solutions are possible for both Deborah numbers in the entire cavity except in the local neighbourhood of the points A and B (where the stationary wall meet the lid). Even at $De = 0.2$, in the small neighbourhood of

Copyright © 2006 John Wiley & Sons, Ltd.

the points A and B solutions do not yield a limit point and the element residuals I^e remain relatively high indicating that the GDEs are not satisfied accurately in these regions. This local zone grows with increasing Deborah number. At $De = 0.4$ this zone is significantly larger compared to $De = 0.2$. Progressively increasing values of *De* propagate this zone into progressively larger portion of the cavity and eventually contaminate the solution in the whole cavity. Graphs of $\dot{\gamma}$ for $De = 0.2$ and 0.4 clearly show that only in relatively small portion of the cavity away from the moving lid $\dot{\gamma}$ values are within the permissible range for Oldroyd-B model confirming the lack of validity of Oldroyd-B model for the majority of flow domain of the cavity. However, excessively high values of $\dot{\gamma}$ alone are not responsible for the inability of the simulations to yield limit points. Oldroyd-B model lacks physics of two-dimensional elasticity and hence produces erroneous elastic stresses which contaminate all other quantities as well. Increasing Deborah numbers result in increasing elastic stresses that are erroneous and eventually result in total failure of the numerical simulation process. Values of $\dot{\gamma}$ beyond the range of validity of the Oldroyd-B model accelerate the generation of spurious solution due to the fact that high $\dot{\gamma}$ values correspond to high velocity gradients and thus increased spurious elastic stresses which contaminate other flow quantities as well.

(9) As observed in the published literature, insistence to compute with Oldroyd-B model for higher Deborah numbers is not meaningful when we know fully well that Oldroyd-B model is only applicable for relatively low strain rates. For low values of $\hat{\dot{\gamma}}$ producing low elastic stresses, one could perhaps tolerate the erroneous behaviour of the model in the direction normal to the applied stress. However, for most practical problems of interest such as cavity, sudden expansion, sudden contraction, stick-slip, etc. the localized zones of high $\hat{\dot{\gamma}}$ is a reality. In such cases simulations using Oldroyd-B model for flow rates of practical interest: (i) may not be possible and (ii) even if possible, are sure to yield erroneous results.

(10) It is significant to note that, the mathematical framework and least squares computational process based on *h*, *p*, *k* utilized here is free of inherent and numerical diffusion [40] and that the upwinding techniques such as SUPG, SUPG/DC, SUPG/DC/LS and their many variations are neither needed nor used in the present work. Furthermore, various methods such as elastic-viscous decomposition of stress, EEME, EEME/SUPG, EVSS/SUPG, etc. though may show some benefits in Galerkin methods with weak form, but are of little or no consequence in the present computational framework due to the fact that regardless of the nature of GDEs, least squares processes are always VC. Since, the GDEs are always non-linear, Galerkin method with weak form is always VIC and hence the resulting computational processes always have the possibility of the spurious numerical solutions. The computations for any $De \neq 0$ are undoubtedly erroneous due to the tact that the constitutive model fails to incorporate correct physics of two-dimensional elasticity, hence computations for higher *De* are of very little consequence. The failure of the computational process depends upon the extent to which elastic stresses are erroneous and exceeding $\hat{\dot{\gamma}}$ beyond the range of validity of the constitutive model, is certainly a major contributing factor in progressively erroneous computations for progressively increasing Deborah numbers and eventual failure of the computations, i.e. lack of convergence of the Newton's method with line search.

Copyright © 2006 John Wiley & Sons, Ltd.

ACKNOWLEDGEMENTS

This research work has been sponsored by grants from DEPSCOR, AFOSR and WPAFB under grant numbers F 49620-03-1-0298 and F 49620-03-1-0201. The support provided by first and third authors endowed professorship funds is also greatly appreciated. The computational facilities provided by the computational mechanics laboratory of the Department of Mechanical Engineering of the University of Kansas is also acknowledged.

REFERENCES

1. Richards GD, Townsend P. A finite element computer model of the hole pressure problem. *Rheologica Acta* 1981; **20**:261–269.
2. Cochrane T, Walters K, Webster MF. Newtonian and non-Newtonian flow near a re-entrant corner. *Journal of Non-Newtonian Fluid Mechanics* 1982; **10**:95–114.
3. Tiefenbruck G, Leal LG. A numerical study of the motion of a visco-elastic fluid past rigid spheres and spherical bubbles. *Journal of Non-Newtonian Fluid Mechanics* 1982; **10**:115–155.
4. Richards GD, Townsend P. Computer modeling of flows of elastic liquids through complex vessels and with forced convection. *Journal of Non-Newtonian Fluid Mechanics* 1982; **10**:175–183.
5. Jackson KP, Walters K, Williams RW. A rheometric study of Boger fluids. *Journal of Non-Newtonian Fluid Mechanics* 1984; **14**:173–188.
6. Dupret F, Marchal JM, Crochet MJ. On the consequence of discretization errors in the numerical calculation of visco-elastic fluid. *Journal of Non-Newtonian Fluid Mechanics* 1985; **18**:173–186.
7. Phan Thein N, Dudek J, Boger DV, Tirtaatmadja V. Squeeze film flow of ideal elastic liquid. *Journal of Non-Newtonian Fluid Mechanics* 1985; **18**:227–254.
8. Binnington RJ, Boger DV. Constant viscosity elastic liquids. *Journal of Rheology* 1985; **29**(6):887–904.
9. Phan Thein N, Khan MMK. Flow of an Oldroyd-type fluid through a sinusoidally corrugated tube. *Journal of Non-Newtonian Fluid Mechanics* 1987; **24**:203–220.
10. Stergios P, Beris AN. Calculation of steady-state viscoelastic flow in an undulating tube. *Journal of Non-Newtonian Fluid Mechanics* 1989; **31**:231–287.
11. Zheng R, Phan Thein N, Tanner RI. On the flow past a sphere in cylindrical tube limiting Weissenberg number. *Journal of Non-Newtonian Fluid Mechanics* 1990; **36**:27–49.
12. Jung YY, Yang N. A numerical study of the planar contraction flow of a viscoelastic fluid using the SIMPLER algorithm. *Journal of Non-Newtonian Fluid Mechanics* 1991; **39**:89–106.
13. Stergios P, Beris AN. Viscoelastic flow in an undulating tube. Effects of high elasticity, large amplitude of undulation and inertia. *Journal of Non-Newtonian Fluid Mechanics* 1991; **39**:375–405.
14. Stergios P, Beris AN. Pseudospectral calculations of viscoelastic flow in periodically constricted tube. *Computational Methods in Applied Mechanical Engineering* 1992; **98**:307–328.
15. Becker LE, Mckinley GH, Rasmussen HK, Hassager O. The unsteady motion of a sphere in a viscoelastic fluid. *Journal of Rheology* 1994; **38**(2).
16. Keiller RA. Entry-flow calculations for Oldroyd-B and FENE equations. *Journal of Non-Newtonian Fluid Mechanics* 1993; **46**:143–178.
17. Davis AR, Devin J. On corner flow of Oldroyd-B fluid. *Journal of Non-Newtonian Fluid Mechanics* 1993; **50**:173–191.
18. Saramito P. A new θ-algorithm and incompressible FEM for viscoelastic fluid flow. *Mathematical Modelling and Numerical Analysis* 1994; **28**(1):1–34.
19. Hulsen MA, Van Heel APG, Van den Brule BHAA. Simulation of viscoelastic flows using Brownian configuration fields. *Journal of Non-Newtonian Fluid Mechanics* 1997; **70**:79–101.
20. Eggleton CD, Pulliam TH, Ferziger JH. Numerical simulation of viscoelastic flow using flux difference splitting at moderate Reynolds number. *Journal of Non-Newtonian Fluid Mechanics* 1996; **64**:269–298.
21. Xue SC, Phan Thein N, Tanner RI. Three-dimensional simulations of viscoelastic flows through planar contractions. *Journal of Non-Newtonian Fluid Mechanics* 1998; **74**:27–45.
22. Yuriko R, Olgunju DO. Inertial effection stability of cone and plate flow. Part 2: non-axisymmetric modes. *Journal of Non-Newtonian Fluid Mechanics* 1998; **78**:27–45.
23. Oliviera PJ, Piho FT, Pinto GA. Numerical simulation of non-linear elastic flows with a general collocated finite volume method. *Journal of Non-Newtonian Fluid Mechanics* 1998; **79**:1–43.
24. Wang B, Sun C, Zhao LYZ. Numerical simulation of planar 4:1 contraction flow of viscoelastic fluid using higher order upwind method. *Tsinghua Science and Technology* 2000; **5**(1):54–59.
25. Surana KS, Ahmadi AR, Reddy JN. *k*-Version of finite element method for self-adjoint operators in BVP. *International Journal of Computational Engineering Science* 2002; **3**(2):155–218.

Copyright © 2006 John Wiley & Sons, Ltd.

26. Surana KS, Ahmadi AR, Reddy JN. *k*-Version of finite element method for non-self-adjoint operators in BVP. *International Journal of Computational Engineering Science* 2003; **4**(4):737–812.
27. Surana KS, Ahmadi AR, Reddy JN. *k*-Version of finite element method for non-linear differential operators in BVP. *International Journal of Computational Engineering Science* 2004; **5**(1):133–207.
28. Bird RB, Amstrong RC, Hassager O. *Dynamics of Polymeric Liquids*, vol. 1. Wiley: New York, 1987.
29. Surana KS, Bhola S, Reddy JN, Tenpas PW. *k*-Version of finite element method in 2-D polymer flows: Maxwell model. *International Journal for Numerical Methods in Engineering* 2005, in review.
30. Dilip R, Armstrong RC, Brown RA. Comparison of computational efficiency of flow simulations with multi-mode constitutive equations: integral and differential models. *Journal of Non-Newtonian Fluid Mechanics* 1993; **75**:243–273.
31. Surana KS, Rajwani A, Reddy JN. *k*-Version of finite element method in singular boundary value problems: linear elastic fracture mechanics. *Computational Methods in Engineering Science and Mechanics* 2005, in press.
32. Surana KS, Petti SR, Ahmadi AR, Reddy JN. *p*-Version hierarchical interpolation functions for higher order continuity finite element models. *International Journal of Computational Methods in Engineering Science and Mechanics* (formerly, *International Journal of Computational Engineering Science*) 2001; **2**(4):357–382.
33. Surana KS, Gupta P, Reddy JN, Tenpas PW. h, p, k least squares finite element processes for 1-D Helmholtz equation. *Computational Methods in Engineering Science and Mechanics* 2005, in press.
34. Surana KS, Gupta P, Reddy JN, Tenpas PW. h, p, k least squares finite element processes for 2-D Helmholtz equation. *Computational Methods in Engineering and Mechanics* 2005, (to be submitted).
35. Gelfand IM, Fomin SV. *Calculus of Variations*. Dover: New York, 2000.
36. Mikhlin SG. *Variational Methods in Mathematical Physics*. Pergamon Press: New York, 1964.
37. Reddy JN. *Functional Analysis and Variational Methods in Engineering*. McGraw-Hill: New York, 1986.
38. Boger DV, Hur DU, Binnington RJ. Further observation of elastic effects in tubular entry flow. *Journal of Non-Newtonian Fluid Mechanics* 1986; **20**:31–49.
39. Christine B, Crochet MJ. The time dependent flow of a viscoelastic fluid around a sphere. *Journal of Non-Newtonian Fluid Mechanics* 1994; **54**:303–329.
40. Surana KS, Sandhu JS. Investigation of diffusion in *p*-version LSFE and STLSFE formulations. *Computational Mechanics* 1995; **16**:151–169.

Copyright © 2006 John Wiley & Sons, Ltd.